1

2

Estimating nitrogen and sulfur deposition across China

during 2005-2020 based on multiple statistical models

5

6   Kaiyue Zhou[1], Wen Xu[3], Lin Zhang[4], Mingrui Ma[1], Xuejun Liu[3], Yu Zhao[1,2*]

7

8 1. State Key Laboratory of Pollution Control & Resource Reuse and School of the
9 Environment, Nanjing University, Nanjing, Jiangsu 210023, China

10 2. Jiangsu Collaborative Innovation Center of Atmospheric Environment and
11 Equipment Technology (CICAEET), Nanjing University of Information Science &
12 Technology, Nanjing, Jiangsu 210044, China

13 3. Key Laboratory of Plant-Soil Interactions of MOE, College of Resources and
14 Environmental Sciences, National Academy of Agriculture Green Development, China
15 Agricultural University, Beijing 100193, China

16 4. Laboratory for Climate and Ocean-Atmosphere Sciences, Department of
17 Atmospheric and Oceanic Sciences, School of Physics, Peking University, Beijing
18 100871, China

19

20 *Corresponding author: Yu Zhao

21 Phone: 86-25-89680650; email: yuzhao@nju.edu.cn

22

23   **Abstract**

24   Due to the rapid development of industrialization and substantial economy, China

25   has become one of the global hotspots of nitrogen (N) and sulfur (S) deposition

26   following Europe and the USA. Here, we developed a dataset with full coverage of N

27   and S deposition from 2005 to 2020, with multiple statistical models that combine

28   ground-level observations, chemistry transport simulations, satellite-derived vertical

29   columns, and meteorological and geographic variables. Based on the newly developed

30   random forest method, the multi-year averages of dry deposition of oxidized nitrogen

31   (OXN), reduced nitrogen (RDN) and S in China were estimated at 10.4, 14.4 and 16.7

32   kg N/S ha^{-1} yr^{-1}, and the analogous numbers for total deposition were respectively

33   15.2, 20.2 and 25.9 kg N/S ha^{-1} yr^{-1} when wet deposition estimated previously with a

34   generalized additive model (GAM) was included. The dry to wet deposition ratio

35   ($R_{\mathrm{dry/wet}}$) of N stabilized in earlier years and then gradually increased especially for

36   RDN, while that of S declined for over ten years and then slightly increased. The RDN

37   to OXN deposition ratio ($R_{\mathrm{RDN/OXN}}$) was estimated to be larger than 1 for the whole

38   research period and clearly larger than that of the USA and Europe, with a continuous

39   decline from 2005 to 2011 and a more prominent rebound afterwards. Compared with

40   the USA and Europe, a more prominent lagging response of OXN and S deposition to

41   precursor emission abatement was found in China. The OXN dry deposition presented

42   a descending gradient from east to west, while the S dry deposition a descending

43   gradient from north to south. After 2012, the OXN and S deposition in eastern China

44   declined faster than the west, attributable to stricter emission controls. Positive

45   correlation was found between regional deposition and emissions, while smaller

46   deposition to emission ratios (D/E) existed in developed eastern China, attributed to

47   more intensive human activities and thereby anthropogenic emissions.

48   **1. Introduction**

49   Atmospheric deposition of nitrogen (N) and sulfur (S) is considered as a serious

50 environmental problem, leading to widespread ecosystem acidification and

51 eutrophication, as well as human health damages (Baker et al., 1991; Burns et al., 2016;

52 Payne et al., 2011; Reuss et al., 1987; Zhang et al., 2018a). In order to understand the

53 spatial distribution and temporal variability of deposition, long-term observation

54 networks have been established globally particularly in developed countries or regions,

55 such as Clean Air Status and Trends Network/the National Atmospheric Deposition

56 Program (CASTNET/NADP) in the USA (Beachley et al., 2016), Canadian Air and

57 Precipitation Monitoring Network (CAPMoN) in Canada (Cheng et al., 2022),

58 European Monitoring and Evaluation Program (EMEP) in Europe (Simpson et al.,

59 2012), and Acid Deposit Monitoring Network in East Asia (EANET; Tørseth et al.,

60 2012; Totsuka et al., 2005; Yamaga et al., 2021). Reductions of anthropogenic NO_X and

61 SO_2 emissions in North America have been very effective in reducing the oxidized

62 nitrogen (OXN) and wet S deposition (Cheng and Zhang, 2017; Feng et al., 2021;

63 Likens et al., 2021). In the USA, for example, OXN decreased significantly in most

64 areas, while reduced nitrogen (RDN) increased gradually in agricultural areas (Holland

65 et al., 2005; Li et al., 2016). Similarly, the long-term observation in Europe shows a

66 downward trend for N and S deposition over the last two decades (Keresztesi et al.,

67 2019; Theobald et al., 2019).

68   China has become one of global hotspots of atmospheric deposition due mainly to

69 the large anthropogenic emissions from increased industrial economy and energy

70 consumption for the past two decades (Vet et al., 2014). To reduce acid rain and later

71 improve air quality, the Chinese government has enacted a series of policies to cut the

72 emissions of atmospheric deposition precursors since 2005 (Li et al., 2017; Liu et al.,

73 2015; Zheng et al., 2018a), including the policy of limiting national total emission

74 levels of SO_2 and NO_X within the 11th Five-year Plan (FYP, 2006-2010) and 12th FYP

75 period (2011-2015) respectively, the National Action Plan on the Prevention and

76 Control of Air Pollution (NAPPCAP, 2013-2017), and the Three-Year Action Plan to

77 fight air pollution (TYAPFAP, 2018-2020). Estimated by the Multiple-resolution

78   Emission Inventory for China (MEIC, http://www.meicmodel.org), those policies have

79   reduced annual SO_2 and NO_X emissions from 2007 and 2012, respectively (Li, 2020;

80   Wang et al., 2022; Zhang et al., 2019), while the change in NH_3 was relatively small.

81   The SO_2 and NO_X vertical column densities (VCDs) measured from satellite remote

82   sensing have also declined to varying degrees across the country (Krotkov et al., 2016;

83   Xia et al., 2016). Besides emissions and ambient columns, accurate estimation on the

84   changing N and S deposition is crucial for evaluating the effectiveness of national

85   policies on decreasing the ecological risk. Limited by data and methods (explained

86   below), however, few studies have been conducted to link the long-term trend of

87   deposition to the regulations of air pollution prevention.

88   Similar to developed countries, the direct knowledge of deposition in China came

89   first from ground observation. Since 1990s, atmospheric deposition monitoring

90   networks in China have been gradually established and improved, such as the Chinese

91   Nationwide Nitrogen Deposition Monitoring Network (NNDMN; Xu et al., 2019) and

92   the Chinese Ecosystem Research Network (CERN; Fu et al., 2010). They provide

93   essential information for quantifying dry and wet deposition and revealing its long-

94   term variability at site level. For example, Liu et al. (2013) found a significant growth

95   in bulk nitrogen deposition in China between 1980 and 2010 based on meta-analyses of

96   historical observation data. Due to insufficient spatial and temporal coverage, however,

97   data obtained at individual sites could not fully support the analysis of widespread and

98   long-term evolution of deposition and might miss diverse patterns of changing

99   deposition by region (Hou et al., 2019; Lye and Tian, 2007). Statistical methods, which

100   incorporated meteorological and environmental variables with higher temporal and

101   horizontal resolutions and wide coverage in time and space (e.g., satellite-derived

102   VCDs), have been increasingly applied to fill the observation gap. Linear or nonlinear

103   relationship between those variables and observed deposition have been developed and

104   applied for periods and regions without observation (Jia et al., 2016; Xu et al., 2018;

105   Yu et al., 2019). For example, Liu et al. (2017a) and Zhang et al. (2018b) obtained the

106 removal rate of SO_2 and NO_X by precipitation in the whole atmospheric boundary layer

107 through linear regression method, and estimated the wet S deposition in 2005-2016 and

108 nitrogen in 2010-2012 in China. Relatively high uncertainty existed in the simple linear

109 assumption, given the complicated effects of multiple variables (e.g., meteorological

110 conditions and underlying surface types) on deposition. Although advanced statistical

111 methods such as k-Nearest Neighbor (KNN), Gradient Boosting Machine (GBM) and

112 neural networks have been developed to predict the air pollutant concentrations, they

113 are much rarely used in the estimation of deposition (Li et al., 2020b; Li et al., 2019;

114 Qin et al., 2020; Wu et al., 2021). Out of the limited studies, Li et al. (2020a)

115 developed machine learning prediction methods based on multi-sites observation data

116 and integrated meteorological and land use type information, which improved the

117 prediction accuracy of temporal and spatial distribution of ammonium (NH_4^+) wet

118 deposition.

119 Besides spatiotemporal coverage, integrated estimation for multiple species is

120 another great challenge, particularly for dry deposition. Compared with wet or bulk

121 deposition, there are very few data available for direct observation of dry deposition

122 and an "inferential method" that incorporates numerical-simulated dry deposition

123 velocity (V_d) and surface concentration has been commonly applied (Cheng et al., 2012;

124 Luo et al., 2016; Wesely, 1989; Xu et al., 2015; Wen et al., 2020). Notably, there are

125 even fewer studies on the dry deposition of secondary-formation species with neither

126 surface nor satellite observation data available at the regional scale (e.g., nitrate (NO_3^-),

127 NH_4^+, and sulfate (SO_4^{2-})). Chemistry transport modeling (CTM), which takes

128 mechanisms of secondary formation of atmospheric species into account, is able to

129 provide the temporal and spatial distribution of ambient concentration of those species,

130 thus can potentially be incorporated into the machine learning framework to improve

131 the deposition estimation and complete the information for individual species. Such

132 application (combination of CTM and machine learning in deposition estimation) has

133 been seldom reported to our knowledge.

134   In response to the above limitations, this study aims to develop a machine

135   learning framework for estimating the historical long-term deposition of multiple N

136   and S species at relatively high horizontal ($0.25^{o} \times 0.25^{o}$) and temporal resolution

137   (monthly) for China, and to explore the comprehensive impact of the national air

138   pollution controls on the deposition. We select the period 2005-2020, which covers

139   three national FYP periods (11th-13th), NAPPCAP and TYAPFAP. We applied a random

140   forest (RF) method and a generalized additive model (GAM) combining different

141   datasets, including ground-level deposition observation, satellite-derived VCDs,

142   meteorological and geographic variables, and CTM simulation, and explore the

143   spatiotemporal variability of dry and wet deposition for the country. The ratios of

144   deposition to emissions (*D/E*) were then calculated by region and species to illustrate

145   the source–sink relationships of atmospheric pollutants. The outcomes provide

146   scientific basis for further formulating emission control strategies, combining potential

147   ecological risks of deposition.

148   **2. Materials and methods**

149   **2.1 Study domain**

150   We selected Chinese mainland as the research area including 31 provincial-level

151   administrative regions (excluding Hong Kong, Macao and Taiwan). As shown in

152   Figure 1, the 31 provinces are geographically classified into 6 parts, i.e., North Central

153   (NC), North East (NE), North West (NW), South East (SE), South West (SW), and the

154   Tibetan Plateau (TP), representing the diverse social-economical and geo-climatic

155   conditions. The details in climate, population and GDP are provided by region in Table

156   S1 in the Supplement. Basically, NC (with Inner Mongolia excluded) and SE belong to

157   the relatively developed regions in eastern China, NW, SW and NE belong to less

158   developed regions, while TP represents the background region. Bounded by the

159   Qinling Mountain-Huaihe River Line (Figure 1), the climate in the south (SE and SW)

160   is humid with more precipitation than the north (e.g., NC).

161   **2.2 Dry deposition flux estimation**

162   **2.2.1 Random forest (RF) model description**

163   Figure 2 shows the methodology framework of dry and wet deposition simulation.

164   We applied a multisource-fusion RF model to estimate the spatiotemporal pattern of

165   dry deposition for individual N and S species including NO_3^-, HNO_3, NO_2, NH_4^+, NH_3,

166   SO_2, and SO_4^{2-} (H_2SO_4 is not included due to its tiny amount and unavailability of

167   relevant data), at $0.25^o \times 0.25^o$ horizontal resolution and monthly level for 2005-2020.

168   RF model is a state-of-art statistical method to deal with the complicated nonlinear

169   relationship between response variable and interpretation variables. Briefly, with the

170   ensemble learning, the RF regression predictions are determined as the average of the

171   multiple regression trees based on the bootstrap sampling method (Breiman, 2001).

172   The model performance strongly depends on two crucial parameters, *ntree* (number of

173   the regression trees) and *mtry* (number of interpretation variables sampled for splitting

174   at each node), and they were respectively determined at 1000 and 3 to train our model.

175   Not all interpretation variables participate in the process of node splitting (Li et al.,

176   2020b), thus significant correlations of regression trees can be avoided. Besides, the

177   backward variable selection was performed on the RF model to achieve the better

178   performance. Please refer to SI Text Section for the detailed algorithm of the model.

179   We ran the RF modeling program by using the "caret" package in R software

180   (version 4.1.2; Kuhn, 2021). As shown in Figure 2, we firstly applied the inferential

181   method to calculate the dry deposition flux (F_d) at ground observation sites as response

182   variable:

183    $$F_d = C \times V_d \tag{1}$$

184   where C is the estimated (for SO_4^{2-}) or observed concentration (for other species)

185   described in Section 2.2.2, and V_d is the modeled dry deposition velocity (V_d) with the

186   Goddard Earth Observation System-Chemistry (GEOS-Chem) 3-D global transport

187   model described in Section 2.2.4.

188   Secondly, we selected satellite-derived tropospheric VCDs of SO_2, NO_2 and NH_3,

189   surface concentrations of NO_3^-, HNO_3, NH_4^+, and SO_4^{2-} simulated from CTM,

190   meteorological factors, geographic covariates, and emission data as interpretation

191   variables. We used the "nearZeroVar" function in "caret" package to eliminate the zero

192   variance variables, to delete highly correlated variables, and to prevent the

193   multicollinearity. Based on the Recursive Feature Elimination (RFE), we then input the

194   final variables to the model as summarized in Table S2 in the supplement. The RFE

195   algorithm is a backward selection of variables based on the relative importance of

196   interpretation variables (RIV). In order to eliminate the different distributions/ranges

197   caused by the magnitudes of various variables, we mapped them to the same interval

198   through standardization and normalization. Before modeling, the interpretation

199   variables were sorted, and the less important factors were eliminated in turn. The RF

200   model captured the nonlinear relationship between the dry deposition (F_d) and

201   interpretation variables:

202
$$F_d = \frac{1}{N}\sum_{n=1}^{N}\{\theta(VCDs) + \theta(Mete) + \theta(Emi) + \theta(Geo) + \theta(CTM)\} \qquad (2)$$

203   where N is the number of samples; θ is the random vector; *Mete*, *Emi*, *Geo* and *CTM*

204   represents the meteorology factors, emission data, geography and surface

205   concentrations simulated from CTM, respectively.

206   Finally, we split the entire model fitting dataset into 10 groups to test the

207   robustness of RF model (10-fold cross validation). In each round of cross validation,

208   the samples in 9 groups were used as the training data, and the remaining group was

209   applied for prediction. This process repeated 10 times and every group was tested. The

210   consistency between the calculated F_d (as an observation) and predictions was

211 evaluated using statistical indicators, including coefficient of determination (R^2), root

212 mean squared prediction error (RMSE), mean prediction error (MPE) and relative

213 prediction error (RPE).

214 **2.2.2 Ground-level concentration observations and prediction**

215 The daily ground-level concentrations of NO_2 and SO_2 during 2013-2020 were

216 obtained from the real-time data publishing system of the China National

217 Environmental Monitoring Centre (CNEMC,

218 http://datacenter.mee.gov.cn/websjzx/queryIndex.vm), with the abnormal values

219 eliminated. The total number of observation sites reached 1532 in 2020, mainly located

220 eastern China with dense industrial economic and population (e.g., 600 and 408 sites in

221 SE and NC, respectively), as shown in Figure 1. Monthly-level concentrations were

222 then calculated for RF model prediction. The Nationwide Nitrogen Deposition

223 Monitoring Network (NNDMN) established by China Agricultural University contains

224 43 monitoring sites in China (as shown in Figure 1) and measured monthly

225 concentrations gaseous NH_3, NO_2, and HNO_3 and particulate NH_4^+ and NO_3^- in air

226 from 2010 to 2014. The NH_3, HNO_3, NH_4^+ and NO_3^- concentrations were measured

227 using the DELTA active sampling systems (DEnuder for Long-Term Atmospheric

228 sampling), while NO_2 samples were collected with Gradko passive diffusion tubes

229 deployed in duplicate or triplicate. The empirically determined effective size cut-off for

230 aerosol sampling was of the order of 4.5 µm (Flechard et al., 2011). The complete

231 datasets of NNDMN were published in previous work (Xu et al., 2019).

232 Due to the lack of large-scale ground observation data, SO_4^{2-} concentrations were

233 obtained with an indirect method, according to the strong association between SO_2 and

234 SO_4^{2-} (Luo et al., 2016). We simulated SO_2 and SO_4^{2-} concentrations for 2013-2020

235 with CTM, and developed the relationships between the two with GAM for each year.

236 The SO_4^{2-} concentrations were then calculated based on the observed SO_2

237 concentrations from CNEMC and the relationships between SO_2 and SO_4^{2-}:

$$238 \qquad C_{SO_4^{2-}} = C_{SO_2} \times f(C_{CTM-SO_4^{2-}}, C_{CTM-SO_2}) \qquad\qquad (3)$$

239   where C_{SO_2} is the monthly ground-level concentration at CNEMC for each year of

240   2013-2020; $C_{CTM-SO_4^{2-}}$ and C_{CTM-SO_2} are the SO_4^{2-} and SO_2 concentrations simulated

241   by CTM for each year of 2013-2020 (see Section 2.2.4 for CTM description),

242   respectively; and f is the relationship between SO_4^{2-} and SO_2 obtained from GAM. As

243   shown in Figure S1 in the Supplement, significant positive correlations were found for

244   SO_4^{2-} and SO_2 concentrations, with the total correlation coefficient (R) estimated at

245   0.86 (p<0.001) for 2013-2020.

246   **2.2.3 Satellite-derived VCDs**

247   The tropospheric VCDs of NO_2 from 2005 to 2020 were taken from Peking

248   University OMI NO2 tropospheric product version2 (POMINO v2; Liu et al., 2019),

249   based on the observation of Ozone Monitoring Instrument (OMI). The VCDs with

250   cloud coverage over 25% were eliminated as high cloudiness would distort satellite

251   detection and increase inversion error. The daily SO_2 VCDs were obtained from Level-

252   3e   OMSO2   Data   Products   from   2005   to   2020

253   (https://disc.gsfc.nasa.gov/datasets/OMSO2e_003/summary). All the OMI SO_2 data

254   were generated by an algorithm based on principal component analysis (PCA), which

255   was considerably sensitive to anthropogenic emissions (Krotkov et al., 2016). The total

256   VCDs of NH_3 were derived from the Infrared Atmospheric Sounding Interferometer

257   (IASI), board on MetOp-A platform. The standard daily IASI/Metop-A ULB-LATMOS

258   total column Level-2 product v2.2.0 is available from 2008 to 2020 (https://iasi.aeris-

259   data.fr/nh3_iasi_a_arch/). The daily total column was excluded when the cloud

260   coverage was >25%, the relative error was >100%, or the absolute error was $>5\times10^{15}$

261   molecules cm^{-2} (Whitburn et al., 2016). The NH_3 VCDs from 2005 to 2008 were

262   estimated based on the linear correlations between NH_3 emission and VCDs during

263   2008-2020.

264   We used the Kriging interpolation method to fill the missing values, and obtained

265   the spatial pattern of VCDs at the horizontal resolution of 0.25°×0.25°. Monthly-level

266   VCDs were calculated based on the daily products from 2005 to 2020.

267   **2.2.4 CTM model description**

268   We used GEOS-Chem v12.1.1 (http://geos-ch em.org) to simulate the V_d and the

269   ground-level concentrations of individual species. The GEOS–Chem model is a global

270   3-D model of atmospheric composition driven by assimilated meteorological

271   observations from the GEOS of the NASA Global Modeling and Assimilation Office.

272   It is a state-of-the-art, comprehensive, easily accessible global atmospheric

273   composition model that has been widely applied around the world to advance the

274   understanding of human and natural impacts on the atmospheric environment (Bey et

275   al., 2001; Park, 2004; Eastham et al., 2018). A nested version was applied with the

276   native horizontal resolution of 0.5°×0.625° over East Asia (70-150°E, 11°S-55°N) and

277   4°×5° for rest of the world, and the simulated V_d and concentrations within China were

278   spatially interpolated at the resolution of 0.25°×0.25°. The V_d for 2013-2020 was

279   calculated based on a standard big-leaf resistance-in-series parameterization as

280   described by Wesely (1989) for gases and Zhang et al. (2001) for total particles, and

281   applied in estimation of the response variable dry deposition flux. The detailed

282   calculation process is described in the Text Section in the supplement, and the annual

283   averages of V_d for different species are presented by land use type in Table S3 in the

284   supplement. The simulated concentrations of individual species (NO_3^-, HNO_3, NH_4^+,

285   and SO_4^{2-}) during 2005-2020 were used as the interpretation variable in RF. The

286   simulated concentrations were in good agreement with the ground measurements, with

287   the correlation coefficients ranging between 0.51 and 0.82 and the normalized mean

288   biases within 30% (Chen et al., 2021).

289   The model was driven by the MERRA-2 assimilated meteorological data provided

290   by the Global Modeling and Assimilation Office (GMAO) at the National Aeronautics

291   and Space Administration (NASA). Meteorology fields such as vertical pressure

292   velocity, temperature, surface pressure, relative and specific humidity had a temporal

293   resolution of 3 h, and surface variables (such as sea level pressure, tropopause pressure)

294   and mixing depths were at 1 h resolution. The model had 47 vertical layers from

295   surface to 0.01 hPa, and the lowest layer is centered at 58 m above sea level.

296   Emissions in GEOS-Chem were processed through Harvard–NASA Emission

297   Component (HEMCO; Keller et al., 2014). We used the Community Emissions Data

298   System for global anthropogenic emissions, overwritten by the regional emissions

299   inventories in the USA, Europe, Canada and Asia, involving the National Emissions

300   Inventory from EPA (NEI; https://www.epa.gov/air-emissions-inventories/air-pollutant-

301   emissionstrends-data), European Monitoring and Evaluation Programme emissions

302   (EMEP; European Monitoring and Evaluation Programme; www.emep.int/index.html)

303   and the MIX inventory that included MEIC over China. Natural NO_X sources from soil

304   and lightning were also included (Lu et al., 2021).

305   **2.2.5 Other data**

306   The meteorological parameters for 2005-2020, including precipitation, boundary

307   layer height, temperature at two meters, wind speed, wind direction, surface pressure,

308   total column, total column ozone, were downloaded from the European Centre for

309   Medium-Range   Weather   Forecasts   (ECMWF,

310   https://apps.ecmwf.int/datasets/data/interim-full-daily/levtype=sfc/) at the resolution of

311    $0.25° \times 0.25°$.

312   Land-Use and Land-Cover Change (LUCC), Digital Elevation Model (DEM),

313   population density data (POP) and Gross Domestic Product (GDP) were obtained from

314   Chinese Resource and Environment Data Cloud Platform (http://www.resdc.cn/).

315   Except for the DEM, other data were compiled at a five-year interval (2005, 2010 and

316   2015 for this study). LUCC was generated by manual visual interpretation of Landsat

317 TM/ETM remote sensing image. We calculated the area fractions of different land use

318 in the buffer zone (60 km in diameter around each site). The elevation spatial

319 distribution data (DEM) were extracted from the Shuttle Radar Topography Mission at

320 the 1-km resolution, assuming no variability during the study period. For GDP and

321 POP, datasets with 1-km resolution were developed through spatial interpolation,

322 taking their spatial interactions with land use type and night light brightness into

323 account (Xu, 2017). Linear interpolation was applied to complete the information for

324 all the years within the research period, and all the above-mentioned interpretation

325 variables were resampled to a uniform horizontal resolution of 0.25°×0.25°.

326 **2.3 Wet deposition flux estimation**

327 As shown in Figure 2, we applied a nonlinear Generalized Additive Model (GAM)

328 developed in our previous work (Zhao et al., 2022) to estimate the monthly wet

329 deposition of SO_4^{2-}, NO_3^- and NH_4^+ in China at a horizontal resolution of 0.25°×0.25°.

330 This model considered the linear and nonlinear correlations between the response

331 variable (referred to as wet deposition in this study) and the selected interpretation

332 variables (satellite-derived VCDs, meteorological factors and geographic covariates,

333 etc.). If there is no strict linear assumption, the likelihood estimate of the wet

334 deposition was the sum of the smooth function of the interpretation variables:

335
$$g(\mu_m) = \sum_{i=1}^{n} f_i(x_{i,m}) + \sum_{p,q} f_{pq}(x_{p,m}, x_{q,m}) + X_m\theta + \varepsilon_m \qquad (4)$$

336 where g is the "link" function, which specifies the relationship between the response

337 variable μ and the linear formulation on the right side of equation; $f_i(x_i)$ is the nonlinear

338 smooth function that explores the single effect of individual interpretation variable x_i;

339 m indicates the month; n represents the total number of interpretation variables for

340 which single effect was considered in the model; $f_{pq}(x_p, x_q)$ is nonlinear smooth

341 function that explores the interaction effect of interpretation variable x_p and x_q; $X\theta$

342 represents an ordinary linear model component for interpretation variables (elements of

343 the vector *X*) not subject to nonlinear transformations; and ε represents the residuals of

344 models. The smooth functions $f_i(x_i)$ and $f_{pq}(x_p, x_q)$ are fitted by thin-plate regression

345 splines and tensor product smoothing, respectively. With an assumption of normal

346 distribution, Gaussian distribution and the log link function are applied for the model

347 residuals.

348   For SO_4^{2-}, the observation data of monthly wet deposition were collected from the

349 East Asia Acid Deposition Monitoring Network (EANET) as response variables. For

350 NO_3^- and NH_4^+, the observed monthly bulk deposition collected by the rain gauges at

351 NNDMN served as the response variables. For all the three species, the interpretation

352 variables contained the precipitation, satellite-derived VCDs, $PM_{2.5}$ concentrations,

353 total column liquid water, temperature, boundary layer height, forest-cover and urban-

354 cover. The data sources and model performance evaluation were described in Zhao et

355 al. (2022). Overall, the 10-fold cross validation R^2 for NO_3^-, NH_4^+ and SO_4^{2-} reached

356 0.51, 0.60, and 0.71, respectively, implying the model well captured the spatiotemporal

357 patterns of wet deposition. Although bulk deposition includes a small amount of dry

358 deposition, the deposition in precipitation obtained through GAM was uniformly

359 defined as wet deposition in this work.

3. Results and discussions

360

3.1 RF model prediction performance

361

362   The RF model performances for dry deposition estimation evaluated with 10-fold

363 cross validation are shown in Figures S2 and S3 in the supplement based on CNEMC

364 and NNDMN, respectively. The multi-year average R^2 of N and S species over China

365 were all above 0.7 and the RMSE of all models were less than 1 kg N/S ha^{-1} yr^{-1}

366 except for NO_2 (1.09 kg N ha^{-1} yr^{-1}) and SO_2 (6.46 kg S ha^{-1} yr^{-1}), indicating the

367 satisfying consistency between observation and prediction. However, the model tended

368 to underestimate the high deposition and overestimate the low one possibly because the

369 model algorithm based on the average of all regression trees resulted in relatively weak

370 estimation of the extreme values. The modeling prediction performance of OXN (NO_3^-,

371 HNO_3 and NO_2) was better than that of RDN (NH_4^+ and NH_3) and S (SO_2 and SO_4^{2-}).

372 For example, the R^2 of NO_2, NO_3^- and HNO_3 were 0.87, 0.73 and 0.78, while those of

373 NH_3 and NH_4^+ were 0.71 and 0.65. POMINO, which reduced the bias of the default

374 product by the OMI Nitrogen Dioxide Algorithm Team (Krotkov et al., 2019; Liu et al.,

375 2019), was demonstrated to be satisfyingly applicable in OXN deposition prediction

376 for China. In addition, the prediction performances of CNEMC were better than those

377 of NNDMN (except for SO_2), attributed partly to much more monitoring stations for

378 the former. As indicated in our previous work, improved model performance could be

379 expected along with the increased abundance of observation data (Zhou et al., 2021).

380   To evaluate the long-term average deposition from RF modeling, we collected 34

381 studies that quantified the deposition of different species and forms (dry or wet) for

382 China using observational, geostatistical or modal methods (Table S4 in the

383 supplement). As shown in Figure 3, gaseous NH_3 and SO_2 were identified as the

384 species with largest dry deposition, while SO_4^{2-} as the species with the largest wet

385 deposition. The multi-year averages (2005-2020) of dry deposition for different species

386 estimated in this study were within the range between 25th Quantile (Q1) and 75th

387 Quantile (Q3) of selected studies except for NH_3 (Figure 3a), but that of SO_4^{2-} wet

388 deposition closing to Q1 was basically lower compared to existing studies (Figure 3b).

389 Most of the existing studies reported SO_4^{2-} wet deposition in China for 2001-2005

390 when the national control of SO_2 emissions and acid rain was still in its initial stage,

391 while limited data was available for more recent years when sharp declines were found

392 for SO_2 emissions. Therefore, the average of existing studies might potentially

393 overestimate the actual average level of S deposition across the country. Overall, the

394 total deposition of N and S from RF modeling was satisfyingly closed to the median

395 level of the existing studies (Figure 3c), indicating the robustness of deposition

396 estimation.

397   We calculated the shares of different forms and species to the average of national

398 total deposition in 2005-2020 (Figure 4). The dry deposition of N followed an order of

399 $NH_3 > HNO_3 > NO_2 > NH_4^+ > NO_3^-$, while the wet NH_4^+ deposition was larger than NO_3^-.

400 As a whole, RDN (58%) was found to contribute more than OXN (42%) to the total N

401 deposition. Those proportions to total N deposition are close to those of emissions, i.e.,

402 54% and 46% for NH_3 and NO_X, respectively (the national emissions of NO_X and NH_3

403 were estimated at 7.2 and 8.3 TgN/yr in MEIC for 2005-2020, respectively). For S

404 species, the dry deposition of SO_2 was over ten times of SO_4^{2-}, while the latter was

405 only species of wet deposition. Dry deposition was estimated to be higher than wet for

406 both N and S, with its fraction in total deposition reaching 70% and 65% within the

407 research period, respectively. The more specific interannual variability and spatial

408 distribution for different forms will be described in Sections 3.2 and 3.3.

409 **3.2 Temporal variability in N and S deposition**

410   Based on the newly developed RF method, the average dry deposition of OXN,

411 RDN, total N and S in China were estimated at 10.4, 14.4, 24.9 and 16.7 kg N/S ha^{-1}

412 yr^{-1} from 2005 to 2020, respectively. The total deposition reached 15.2, 20.2, 35.4 and

413 25.9 kg N/S ha^{-1} yr^{-1}, respectively, when the average wet deposition estimated with

414 GAM (Zhao et al., 2022) was included. Figure 5a-d illustrates the long-term

415 interannual variability of dry and wet deposition for OXN, RDN, total N and S,

416 respectively. Different temporal trends are found for N and S, due partly to the diverse

417 of their precursor emissions. As indicated by MEIC, China's NO_X emission control was

418 limited till 2010, allowing annual national emissions to grow 49% from 2005 to 2012

419 (Figure 5f). The country required installation of selective catalyst reduction (SCR)

420 systems from 2011, and NAPPCAP drove fast growing penetration of SCR in the

421 power and cement production sectors, resulting in a 28.6% reduction in the annual total

422 emissions of NO_X from 2013 to 2020 (Karplus et al., 2018; Li et al., 2018). Similar

423 temporal variability was found for OXN deposition: it was increasing slightly from

424 14.7 in 2005 to 15.7 kg N ha^{-1} yr^{-1} in 2012, and then declining to 14.5 kg N ha^{-1} yr^{-1}

425 in 2020 (Figure 5a). The interannual variation in NH_3 emissions has been much smaller

426 than NO_X, with a slight reduction by 9% from 2005 to 2020 (Figure 5f), attributed to

427 the changes in Chinese agricultural practices, e.g., improved waste management in

428 livestock farming and replacement of highly volatile ammonium bicarbonate with urea

429 in fertilizer types (Liu et al., 2017b; Zheng et al., 2018b). However, the big emission

430 abatement of acidic gases like SO_2 after 2013 was recognized to reduce the sink of NH_3

431 in the atmosphere and to increase of gas-phase NH_3 concentrations (Liu et al., 2018),

432 resulting in more dry NH_3 deposition (Figure 5b). After 2015, China's RDN deposition

433 became relatively stable, which could be partly explained by the implementation of

434 Zero Increase Action Plan for N fertilizer after 2015 (Liu et al., 2022). As a combined

435 effect of changing emissions and atmospheric conditions, the RDN deposition was

436 estimated to grow from 19.5 in 2005 to 20.6 kg N ha^{-1} yr^{-1} in 2020. China has widely

437 applied flue gas sulfurization (FGD) in the power sector since 2005, and has expanded

438 its application to other industries (such as sintering furnaces and non-electric coal-fired

439 boilers) since 2013, as a part of NAPPCAP (Zheng et al., 2018a). As a result, the

440 annual national SO_2 emissions were estimated to decline by 76% from 2005 to 2020

441 (Figure 5f), and the dry deposition of S by 31% (Figure 5d). The wet deposition was

442 less responsive to emissions than dry deposition, and the growth in precipitation was

443 likely offsetting part of the benefit of emission control on wet deposition (Zhao et al.,

444 2022). The total S deposition was calculated to decline 26%, from 28.8 in 2005 to 21.3

445 kg S ha^{-1} yr^{-1} in 2020.

446 Shown in Figure 5a-d as well is the long-term interannual variability of the dry to

447 wet deposition ratio ($R_{dry/wet}$) during 2005-2020. Mann-Kendall test (Ahmad et al.,

448 2015; Comero et al., 2014) was applied to evaluate the significance of $R_{dry/wet}$ trend for

449   N and S, as shown in Table S5 in the supplement. The $R_{dry/wet}$ of N species kept

450   relatively stable for earlier years and then slightly increased since 2015, with the multi-

451   year average ratios estimated at 2.2, 2.5 and 2.4 for OXN, RDN and total N,

452   respectively. The $R_{dry/wet}$ of S declined significantly before 2015 and then slightly

453   increased afterwards, with the average ratio estimated at 1.8 for 2005-2020. The

454   growth of $R_{dry/wet}$ of RDN could be partly attributed to the improved control of acid

455   precursor emissions for recent years. Since 2013, as mentioned above, implementation

456   of NAPPCAP and abatement of SO_2 emissions has reduced the sink of NH_3 in the

457   atmosphere, elevating the free ammonia in the air and thereby $R_{dry/wet}$ of RDN.

458   Significant negative correlation coefficient between precipitation and $R_{dry/wet}$ was found

459   for both OXN (-0.63) and S (-0.64), indicating the influence of precipitation. Notably,

460   precipitation increased at a rate of 6.3 mm yr^{-1} in China during 2005-2015 (Figure S4

461   in the supplement), motivating the formation of wet deposition of SO_2 that is easily

462   soluble in water. Besides, the general growth of air pollutant emissions (excluding SO_2)

463   elevated the atmospheric oxidizing capacity, thereby promoting SO_4^{2-} formation for

464   wet deposition. The declining precipitation after 2015 resulted in the reduced wet

465   deposition and thereby enhanced $R_{dry/wet}$ for OXN and S.

466   Figure 5e shows the long-term interannual variability of the ratio of N to S

467   deposition ($R_{N/S}$) and the ratio of RDN to OXN deposition ($R_{RDN/OXN}$) for different

468   forms during 2005-2020. Growing $R_{N/S}$ was found for most time within the research

469   period, as China started SO_2 emission control earlier than NO_X and NH_3. $R_{RDN/OXN}$

470   indicates the relative contributions of industrial and agricultural activities to N

471   deposition, as the major anthropogenic sources of RDN are animal excrement and

472   fertilizer use in agriculture while those of OXN are fossil fuel combustion in power,

473   industrial and transportation sectors (Pan et al., 2012; Zhan et al., 2015; Zhu et al.,

474   2015). $R_{RDN/OXN}$ is estimated to be larger than 1 for the whole research period, with a

475   continuous decline from 2005 to 2011 and more prominent rebound afterwards, and it

476   reached 1.5 for total N in 2020. The ratio for dry deposition was larger than the wet

477   one. The declining $R_{RDN/OXN}$ before 2011 resulted mainly from the growth of NO_X

478   emissions and thereby OXN deposition, driven by the fast development of industrial

479   economy and increasing fossil fuel combustion. The growing $R_{RDN/OXN}$ since 2012 was

480   expected to be largely driven by the continuous efforts of NO_X emission controls, and

481   highlighted the benefit of those efforts on limiting OXN pollution. Regulation on NH_3

482   emission controls, mainly in agricultural activities, became increasingly important for

483   further alleviating the N pollution.

484   As summarized in Table S6 in the supplement, the annual average deposition of N

485   and S in China was much larger than that for USA estimated by Clean Air Status and

486   Trends Network (CASTNET, https://www.epa.gov/castnet) and National Atmospheric

487   Deposition   Programme   (NADP,   https://nadp.slh.wisc.edu/networks/national-trends-

488   network/) and Europe by European Monitoring and Evaluation Programme (EMEP,

489   https://projects.nilu.no/ccc/index.html). According to Vet et al. (2014), the ensemble-

490   mean results of 21 global CTMs indicated that eastern China was the region with the

491   highest nitrogen deposition in the world, with a value of 38.6 kg N ha^{-1} yr^{-1}. Compared

492   with USA and Europe, China has not only experienced high deposition of N and S but

493   also featured the greatest increase over the past decade (Du and Liu, 2014; Fu et al.,

494   2022; Jia et al., 2016). Figure 6 illustrates the interannual variations of emissions,

495   deposition and $R_{RDN/OXN}$ for China as well as the more developed USA and Europe (28

496   countries). The emission data for the three regions were respectively taken from MEIC,

497   the U.S. Environmental Protection Agency (EPA, https://www.epa.gov/air-emissions-

498   inventories/air-pollutant-emissionstrends-data), and European Environment Agency

499   (EEA, https://www.eea.europa.eu/themes/air). As shown in Figure 6a and 6c, the

500   interannual trends in estimated deposition were basically consistent with those in

501   emissions, with observed reduction for both OXN and S deposition over the USA and

502   Europe. With the slowdown in economic growth and the implementation of air

503 pollution control actions for decades (e.g., Clean Air Act (CAA) in the USA and

504 Convention on Long-range Transboundary Air Pollution (CLRTAP) in Europe), the

505 emissions of NO_X and SO_2 have been reduced by more than 60% and 90% between

506 1980 and 2020, respectively (Constantin et al., 2020; Fowler et al., 2013; Skyllakou et

507 al., 2021; Zhao and Qiao, 2022). However, as a result of the rapidly growing demand

508 for economic development and energy, the fossil fuel consumption and fertilizer

509 utilization increased by 3.2 and 2.0 times during1980-2010 for China, which ultimately

510 led to an increase in the OXN and RDN deposition from 2005 to 2010 (An et al., 2019;

511 Li, 2020; Liu et al., 2020). Following developed countries, gradually tightened

512 measures of reducing SO_2 and NO_X have been launched since 2005 and 2011

513 respectively, and the deposition began to decline afterwards.

514   We selected the periods with fast declines in deposition of OXN and S for the

515 three regions and compared them in Table 1. The relative changes in deposition were

516 smaller than those of emissions for all the regions, and greater declines were found for

517 S for both emissions and deposition than OXN. Compared with Europe and the USA,

518 China had the smallest benefit of precursor emission abatement on deposition. For

519 example, the SO_2 emissions in the USA, Europe and China had been cut by 78.4%

520 (2003-2016), 57.6% (2000-2013) and 75.5% (2007-2020) respectively, while S

521 deposition had declined by 72.5%, 49.9% and 27.0%. This may be caused by a lagging

522 response of deposition to emission abatement, which is more prominent in China.

523 Europe and the USA started emission controls earlier than the selected periods, resulted

524 in a smaller gap between the changes in emissions and deposition afterwards. The

525 comparison implies that the effect of short-term emission reduction in China would not

526 immediately be fully reflected in the deposition. As reported by Yamaga et al. (2021),

527 the trend of NO_3^- to non-sea-salt SO_4^{2-} concentration ratio in precipitation in Japan

528 clearly corresponded to that of the NO_X to SO_2 emission ratio in China. Therefore, the

529 short-term emission reduction in China was likely to reduce the transboundary

530 deposition to downwind areas (such as Japan) sooner. Under this condition, continuous

531 efforts on emission abatement should be made to achieve substantial reduction in

532 domestic deposition and to further mitigate ecological risks. Along with continuous

533 controls of anthropogenic emissions, moreover, the variation of natural sources (e.g.,

534 NO_X from soils) may play a more important role on the changing deposition and

535 deserves more attentions in the future.

536 Figure 6d presents the interannual changes of $R_{RDN/OXN}$ for China, USA, and

537 Europe (28 countries). The $R_{RDN/OXN}$ in China was higher than those in the other two,

538 with an average of 1.3 in 2005-2020 (0.9 and 1.0 for the USA and Europe during the

539 same period). As a developing country, China is an important food producing country

540 in the world, with a long history of agricultural production and planting. Large

541 agricultural production and relatively weak policy management made China the largest

542 NH_3 emissions in the world, leading to a high proportion of RDN deposition to the

543 total N deposition (Kang et al., 2016; Liu et al., 2022). In contrast, in developed USA

544 and Europe with high level of agricultural mechanization and abundant industry and

545 transportation, the relatively high NO_X emissions compared to NH_3 resulted in smaller

546 $R_{RDN/OXN}$ than China.

547 Similar temporal changes in $R_{RDN/OXN}$ can be found for USA and China, i.e.,

548 decline in earlier years and growth afterwards. For USA, the turning point of $R_{RDN/OXN}$

549 occurred in 1999, 13 years earlier than that of China in 2012. The turning points were

550 closely associated with the introduction and implementation of NO_X emission controls

551 for the two countries (CAA Amendments since 1990 for the USA and NAPPCAP since

552 2013 for China). While RDN in China has been the major species since 2005, the OXN

553 in the USA was larger than RDN for over 20 years. The $R_{RDN/OXN}$ kept growing since

554 2000 and exceeded 1 in 2014, indicating a transition of major N species in the

555 deposition. Different from China and the USA, $R_{RDN/OXN}$ in Europe kept declining

556 since 2000, and being smaller than 1 after 2013. In many European countries with

557 abundant agricultural activities (such as Netherlands, Germany, Switzerland and

558 France), the chemical fertilizer and livestock breeding release a large amount of NH_3.

559 Europe attached great importance to the source control of agricultural pollution

560 (though not as strong as for NO_X), adopted the economic guidance method for

561 agricultural environmental subsidies, and member states actively assumed the

562 responsibility for governance for decades (i.e., Common Agriculture Policy, CAP;

563 Zhang et al., 2020). Therefore, the control of NH_3 in Europe was ahead of China,

564 resulting in continuous reduction in NH_3 emissions and thereby $R_{RDN/OXN}$.

565 **3.3 Spatial variability in N and S deposition**

566 Figure 7 shows the spatial distributions of N and S deposition fluxes during 2005-

567 2020. In general, relatively large deposition was found in eastern China with more

568 population and developed industrial economy (e.g., SE and part of NC in Figure 1).

569 Hotspots of dry deposition were commonly located in the north while wet in the south.

570 As a joint effect of concentrations and V_d, high level of OXN dry deposition was

571 estimated in areas with high vegetation cover, such as Yunnan and Fujian province. For

572 S dry deposition, coal-fired boilers for power and heating were intensively distributed

573 in the north, leading to abundant SO_2 emissions and thereby dry deposition.

574 Furthermore, the relatively stable weather conditions with less convection in the north

575 was unfavorable to the dispersion and dilution of pollutants. The emissions were thus

576 liable to be deposited locally. For RDN, the agricultural production, animal husbandry

577 and biomass burning in NC and the northern part of SE led to relatively high NH_3

578 emissions and thereby high dry deposition. The more acidic and humid soils in the

579 south made NH_3 more difficult to release, resulting in lower dry deposition compared

580 to the north. Large wet deposition was mainly found in the south of China associated

581 with the uneven distribution of precipitation. In summer, the air masses in the western

582 Pacific Ocean and the South China Sea were affected by the southeast and southwest

583 monsoon, significantly increasing the rainfall in southeast China. For the total

584 deposition (wet plus dry), the high deposition of OXN and S were located in SE, while

585 RDN and total N were mainly concentrated in NC and the north of SE.

586   As shown in Table S7 in the Supplement, the $R_{\text{dry/wet}}$ of N and S in the eastern

587 China (SE+NC with Inner Mongolia excluded) was smaller than that in western China

588 (NW+TP), attributed mainly to the large precipitation in the former. Given the dry

589 climate and less anthropogenic activities, the pollution was mainly removed from the

590 atmosphere by dry deposition in western regions. The $R_{\text{dry/wet}}$ of TP was the highest out

591 of the six regions, with 2.6 and 3.7 for total N and S, respectively. The $R_{\text{dry/wet}}$ in NE,

592 NW and NC was generally higher than that in the south (SE and SW), resulting also

593 from the abundant precipitation in the south. Higher $R_{\text{RDN/OXN}}$ was found in the west

594 (e.g., NW and TP) and lower in the east (Table S7), as more developed industry in the

595 east resulted in relatively large NO_X emissions and thereby OXN deposition, while

596 farming and animal husbandry shared more in the economy in the west, leading to

597 substantial NH_3 emissions.

598   Figure 8 and Table 2 compare the relative changes of total deposition (wet plus

599 dry) of different species for eastern, western and whole country. The interannual

600 changes of deposition for all species were smaller than that of emissions (Table 2),

601 reconfirming lagging response of deposition to changing emissions as mentioned in

602 Section 3.2. During the period when emissions declined rapidly, the change of

603 deposition has not yet occurred. It should be noted that the emission reduction might be

604 overestimated by MEIC particularly for SO_2 for recent years. Through a "top-down"

605 methodology based on satellite observation, China's SO_2 emissions were estimated to

606 decline 26% from 2011 to 2015 (Qu et al., 2019), slower than the estimation by MEIC

607 at 42%. The relative changes for N and S deposition in eastern China were generally

608 larger than the whole country, indicating the effectiveness of extremely stringent

609 emission controls on those regions with abundant emissions from industrial and traffic

610 sources. The OXN deposition for all the concerned regions shows an invert "V" pattern

611   over time, consistent with the progress of NO_X emissions control (Figure 8a). The

612   relative annual changes in eastern China (9% in 2005-2012 and -12% in 2012-2020)

613   were generally greater than in western (4% in 2005-2012 and -5% in 2012-2020).

614   More specifically, the turning point for western China was later than the East, likely

615   resulting from later implementation of emission control policies. Most measures were

616   first implemented in the highly developed key regions in east and then applied more

617   widely afterwards. As shown in the Figure 8b and Table 2, RDN deposition was

618   relatively stable before 2012, and the temporal changes in eastern and western China

619   were generally consistent with each other. The lack of comparable control policies for

620   NH_3 and strict policy of acid precursors likely explained the increasing trend in RDN

621   afterwards, with 9% in eastern and 10% in western China between 2012 and 2020. The

622   biggest reduction was achieved for S deposition, and the decline in eastern China was

623   faster than that in the western (Figure 8c). Attributable to the earlier and broader use of

624   FGD at coal combustion sources, greater abatement of SO_2 emissions was achieved

625   than NO_X or NH_3 over the past decade, leading to the faster reduction in S deposition

626   than in OXN or RDN (Table 2). In addition, the reduction during 2012-2020 (28%, 18%

627   and 21% for the eastern, western and the whole country, respectively) was clearly

628   larger than that during 2005-2012 (3%, 9% and 7%, respectively), indicating the

629   greatly improved SO_2 controls compared to earlier years.

630   The ratio of deposition to emissions (D/E) is used to analyze the interactions

631   between the pollutant sources and sinks. Figure 9a shows the annual mean D/E ratios

632   during 2005-2020 by species and region. The nationwide D/E of OXN, RDN, and S

633   were 1.4, 2.4, and 2.3, respectively. The D/E in eastern China (e.g., NC and SE) was

634   generally smaller than in western China (NW, SW and TP). The low D/E identified

635   those regions as the major sources of air pollutants due mainly to their intensive

636   emissions, likely influencing air pollution levels in surrounding regions. With less

637   industry, energy consumption and population, by contrast, western China received

638   relatively high deposition compared to local emissions, resulting in large D/E. The very

639   high ratio of D/E indicated that TP was strongly influenced by regional pollution

640   transport. The D/Es of RDN in the six regions were higher than that of OXN and S

641   (except for TP). Due to its relatively short life time, most of NH_3 deposits near the

642   source area, while stronger transport and chemical reaction may occur for NO_X and

643   SO_2 given their longer life time. Significantly positive correlations were found between

644   regional deposition and emissions for all the concern species, with R^2 estimated at 0.81,

645   0.92, and 0.78 for OXN (Figure 9b), RDN (Figure 9c), and S (Figure 9d), respectively.

646   The result implies that the N and S deposition to the six regions were strongly

647   dependent on the spatial pattern of anthropogenic emissions.

648   The annual emissions, deposition and D/E by land use type were displayed in

649   Table S8 in the supplement. High deposition was commonly found in areas with high

650   energy consumption and large emissions, such as urban and construction sites.

651   Associated with different human activities, moreover, the D/E for S and OXN were

652   smaller in urban regions than those in rural ones, whereas that for RDN was slightly

653   larger in urban areas. Transportation and industries resulted in larger NO_X and SO_2

654   emissions in urban locales and agricultural activities enhanced NH_3 in rural ones.

655   Figure 10 shows the spatial distribution of multi-year average deposition by

656   season, which was influenced jointly by varying meteorology and emissions. Basically,

657   larger deposition was found in summer than that in winter, and the seasonal difference

658   was particular bigger for N. The deposition in summer was estimated to be 1.9 and 1.6

659   times in winter for OXN and RDN, respectively, while the ratio was much smaller at

660   1.1 for S. As shown Figure S5 in the Supplement, the V_d of HNO_3 in summer was 4.4

661   times in winter, leading to larger OXN deposition in summer. Moreover, warm weather

662   elevated the volatility of NH_3 in croplands, resulting in greater emissions and thereby

663   deposition in summer. The hotspot of deposition was commonly found in NC and

664   northern SE in summer, while it moved to central SE in winter attributed partly to the

665   prevailing northwesterly wind.

666   **3.4 Uncertainties**

667   Uncertainties existed in current analysis. First, the estimated dry deposition or V_d

668   could not be fully examined with sufficient data from direct observation, attributed

669   mainly to the lack of field measurements. Micrometeorological methods can be used

670   for direct observation of dry deposition, including eddy correlation method, gradient

671   method and relaxation vortex accumulation method. Due to the need for extremely fast

672   response instruments and uniform underlying surfaces, those methods have not yet

673   been widely applied in a long-term and extensive manner. We compared the simulated

674   V_d in this work with other simulation studies in Table S9 in the Supplement. The values

675   from various CTMs are commonly of the same orders for most cases, while big

676   differences exist in some species/land use types, e.g., NO_2 for coastal regions. The bias

677   could be better quantified when more direct observations of V_d get available.

678   Second, error may come from ground-level monitoring data. We collected

679   available data from different monitoring networks, and ignored the difference in

680   observed deposition from diverse methods of sample collection and measurement.

681   Moreover, current RF model relied on the data from observation sites, most of which

682   are located in the eastern China with dense population and developed economy. The

683   model accuracy for remote areas (such as NW and TP) should be further evaluated

684   when more observation data get available for those areas.

685   Third, there was additional uncertainty in the estimation of SO_4^{2-} dry deposition,

686   as there were limited observed ambient concentrations of SO_4^{2-} available for estimation

687   of dry deposition, and CTM had to be applied. The conversion of SO_2 to SO_4^{2-} is

688   influenced by the atmospheric oxidizing capacity, and thereby the NO_X concentration

689   (He et al., 2014; Ye et al., 2023). Along with economic development and

26

690 implementation of air pollution controls, the changing emissions of NO_X as well as

691 some other species (e.g., volatile organic compounds) have altered atmospheric

692 oxidizing capacity within the research period. Using the relationship between 2013 and

693 2020 to extrapolate the SO_4^{2-} deposition for 2005-2020 would potentially bring some

694 uncertainty.

695 Furthermore, bulk deposition obtained from the open precipitation gauge contains

696 part of dry deposition and therefore likely overestimate actual wet deposition. The bias

697 varied by region and was hard to be quantified at the national level. For example, dry

698 deposition was observed to account for around 20% of the bulk at three rural stations in

699 the North China Plain, and the contribution could reach 39% in some urban areas

700 (Zhang et al., 2015; Zhang et al., 2008). In contrast, the difference between bulk and

701 wet deposition of dissolved inorganic nitrogen (DIN) was equal to 12% of the bulk in a

702 rural site in SW (Kuang et al., 2016; Song et al., 2017). Basically, the uncertainty was

703 greater in areas with a higher proportion of dry to total deposition (such as NW and NE

704 areas with less precipitation), and smaller in areas with a lower proportion (such as SE

705 with more precipitation). As SE is the most developed region in China, with relatively

706 high emissions and deposition across the country, the uncertainty from bulk deposition

707 measurement and application is likely of limited impact on the national level or the

708 overall spatial pattern of deposition. Along with continuous development of monitoring

709 networks and increasing availability of deposition data for diverse species, those

710 uncertainties can be further reduced and more accurate deposition estimation can be

711 expected.

4. Conclusions

713 We developed a full N and S deposition dataset for mainland China at the

714 horizontal resolution of 0.25° for 2005-2020, combining the ground-level observations,

715 satellite-derived VCDs, meteorological and geographic information, and CTM. Based

716 on the newly developed RF method, the annual average dry deposition of OXN, RDN

717   and S in China was estimated at 10.4, 14.4 and 16.7 kg N/S ha^{-1} yr^{-1}, while the total

718   deposition reached 15.2, 20.2 and 25.9 kg N/S ha^{-1} yr^{-1}, respectively, with the wet

719   deposition estimated with a GAM model included. The $R_{\text{dry/wet}}$ of N kept relatively

720   stable at the beginning and then gradually increased, especially for RDN, while that of

721   S declined for over 10 years and then slightly increased. Within the whole study period,

722      $R_{\text{RDN/OXN}}$ was estimated to be greater than 1 and clearly larger than that of the USA and

723   Europe, with a continuous decline from 2005 to 2011 and a growth afterwards. The

724   frequent agricultural activities and relatively weak management of manure have

725   resulted in abundant NH_3 emissions and thereby a high proportion of RDN deposition.

726   Improved NO_X emission control was the main reason for the elevated $R_{\text{RDN/OXN}}$ for

727   recent years. Compared with Europe and the USA, China had the smallest benefit of

728   precursor emission reduction on deposition. The prominent lagging response of

729   deposition to emission abatement requires a continuous long-term emission control

730   efforts to substantially reduce atmospheric deposition. As a joint effect of emissions

731   and individual meteorological factors, a downward gradient from east to west was

732   found for dry deposition of OXN while from north to south for S. The wet deposition

733   frequently occurred in the south of China, associated with the spatial distribution of

734   rainfall. The deposition of OXN and S declined faster in eastern China than that in the

735   west after 2012, indicating the effectiveness of extremely strict emission control in

736   developed areas with abundant emissions from industry and transportation. The D/E in

737   eastern China was generally smaller than that in west, as the former was the major

738   sources of air pollutants and the latter received relatively high deposition through

739   regional transport. At the national scale, the deposition strongly depended on the

740   spatial pattern of anthropogenic emissions within the regions. The current study

741   broadens the scientific understanding of China's long-term changes in deposition of

742   typical atmospheric species, as well as the influences of human activities and emission

743   controls. More observation and modeling work is recommended for in-depth analyses

744   on the complicated and changing relationship between emissions and deposition for

745   specific species, as well as the consequent varying effects on ecosystem.

746 **Data availability**

747   The multiyear deposition data by species at the horizontal resolution of 0.25^{o} will be

748   available at http://www.airqualitynju.com/En/Data/List/Datadownload once the paper

749   is published.

750 **Author contributions**

751   KZhou developed the methodology, conducted the research, performed the analyses

752   and wrote the draft. YZhao developed the strategy, designed the research and revised

753   the manuscript. LZhang and MMa provided the support of air quality modeling. WXu

754   and XLiu provided the support of NNDMN data.

755 **Competing interests**

756   The authors declare that they have no conflict of interest.

763 **References**

764   Ahmad I, Tang D,Wang T,Wang M,Wagan B: Precipitation trends over time using

765   Mann-Kendall and Spearman's rho tests in Swat River Basin, Pak. Adv. Meteorol.,

766   431860, https://doi.org/10.1155/2015/431860, 2015.

767   An, Z., Huang, R. J., Zhang, R., Tie, X., Li, G., Cao, J., Zhou, W., Shi, Z., Han, Y., Gu,

768   Z., and Ji, Y.: Severe haze in northern China: A synergy of anthropogenic

769   emissions and atmospheric processes, Proc. Natl. Acad. Sci., 116, 8657-8666,

770   https://doi.org/10.1073/pnas.1900125116, 2019.

771 Baker, L. A., Herlihy, A. T., Kaufmann, P. R., and Eilers, J. M.: Acidic Lakes and
772   Streams in the United States: The Role of Acidic Deposition, Science, 252, 1151-
773   1154, https://doi.org/10.1126/science.252.5009.1151, 1991.

774 Beachley, G., Puchalski, M., Rogers, C., and Lear, G.: A summary of long-term trends
775   in sulfur and nitrogen deposition in the United States: 1990-2013, JSM environ.
776   sci. ecol., 4, 1030-1034, 2016.

777 Bey, I., Jacob, D. J., Yantosca, R. M., Logan, J. A., Field, B. D., Fiore, A. M., Li, Q. B.,
778   Liu, H. G. Y., Mickley, L. J., and Schultz, M. G.: Global modeling of tropospheric
779   chemistry with assimilated meteorology: Model description and evaluation, J.
780   Geophys.   Res.   (Atmos.),   106,   23073-23095,
781   https://doi.org/10.1029/2001jd000807, 2001.

782 Breiman,   L.:   Random   forests,   Mach.   Learn.,   45,   5-32,
783   https://doi.org/10.1023/a:1010933404324, 2001.

784 Burns, D. A., Aherne, J., Gay, D. A., and Lehmann, C. M. B.: Acid rain and its
785   environmental effects: Recent scientific advances, Atmos. Environ., 146, 1-4,
786   https://doi.org/10.1016/j.atmosenv.2016.10.019, 2016.

787 Comero S, Vaccaro S, Locoro G, De Capitani L, Gawlik BM: Characterization of the
788   Danube River sediments using the PMF multivariate approach, Chemosphere, 95,
789   329–335, https://doi.org/10.1016/j.chemosphere.2013.09.028, 2014

790 Chen, Y., Zhang, L., Henze, D. K., Zhao, Y., Lu, X., Winiwarter, W., Guo, Y., Liu, X.,
791   Wen, Z., Pan, Y., and Song, Y.: Interannual variation of reactive nitrogen
792   emissions and their impacts on $PM_{2.5}$ air pollution in China during 2005–2015,
793   Environ. Res. Lett., 16, 125004, https://doi.org/10.1088/1748-9326/ac3695, 2021.

794 Cheng, M., Jiang, H., Guo, Z., Zhang, X., and Lu, X.: Estimating NO_2 dry deposition

795   using satellite data in eastern China, Int. J. Remote Sens., 34, 2548-2565,

796   https://doi.org/10.1080/01431161.2012.747019, 2012.

797   Cheng, I. and Zhang, L.: Long-term air concentrations, wet deposition, and scavenging

798   ratios of inorganic ions, HNO_3 and SO_2 and assessment of aerosol and

799   precipitation acidity at Canadian rural locations, Atmos. Chem. Phys., 17, 4711-

800   4730, https://doi.org/10.5194/acp-17-4711-2017, 2017.

801   Cheng, I., Zhang, L., He, Z., Cathcart, H., Houle, D., Cole, A., Feng, J., O'Brien, J.,

802   Macdonald, A. M., Aherne, J., and Brook, J.: Long-term declines in atmospheric

803   nitrogen and sulfur deposition reduce critical loads exceedances at multiple

804   Canadian rural sites, 2000–2018, Atmos. Chem. Phys., 22, 14631-14656,

805   https://doi.org/10.5194/acp-22-14631-2022, 2022.

806   Constantin, D. E., Bocaneala, C., Voiculescu, M., Rosu, A., Merlaud, A., Roozendael,

807   M. V., and Georgescu, P. L.: Evolution of SO_2 and NO_X emissions from several

808   large combustion plants in Europe during 2005-2015, Int. J. Environ. Res. Public

809   Health, 17, https://doi.org/10.3390/ijerph17103630, 2020.

810   Du, E. and Liu, X.: High rates of wet nitrogen deposition in China: A synthesis, in:

811   nitrogen deposition, critical loads and biodiversity, edited by: Sutton, M. A.,

812   Mason, K. E., Sheppard, L. J., Sverdrup, H., Haeuber, R., Hicks, W. K., Springer,

813   the Netherlands, 49–56, https://doi.org/10.1007/978-94-007-7939-6_6, 2014.

814   Eastham, S. D., Long, M. S., Keller, C. A., Lundgren, E., Yantosca, R. M., Zhuang, J.,

815   Li, C., Lee, C. J., Yannetti, M., Auer, B. M., Clune, T. L., Kouatchou, J., Putman,

816   W. M., Thompson, M. A., Trayanov, A. L., Molod, A. M., Martin, R. V., and Jacob,

817   D. J.: GEOS-Chem High Performance (GCHP v11-02c): a next-generation

818   implementation of the GEOS-Chem chemical transport model for massively

819   parallel applications, Geosci. Model Dev., 11, 2941-2953,

820   https://doi.org/10.5194/gmd-11-2941-2018, 2018.

821   Feng, J., Vet, R., Cole, A., Zhang, L., Cheng, I., O'Brien, J., and Macdonald, A.-M.:

822   Inorganic chemical components in precipitation in the eastern U.S. and Eastern

823   Canada during 1989–2016: Temporal and regional trends of wet concentration and

824   wet deposition from the NADP and CAPMoN measurements, Atmos. Environ.,

825   254, 118367, https://doi.org/10.1016/j.atmosenv.2021.118367, 2021.

826   Flechard, C. R., Nemitz, E., Smith, R. I., Fowler, D., Vermeulen, A. T., Bleeker, A.,

827   Erisman, J. W., Simpson, D., Zhang, L., Tang, Y. S., and Sutton, M. A.: Dry

828   deposition of reactive nitrogen to European ecosystems: a comparison of

829   inferential models across the NitroEurope network, Atmos. Chem. Phys., 11,

830   2703-2728, https://doi.org/10.5194/acp-11-2703-2011, 2011.

831   Fowler, D., Pyle, J. A., Raven, J. A., and Sutton, M. A.: The global nitrogen cycle in

832   the twenty-first century: introduction, Philos. Trans. R. Soc, 368,

833   https://doi.org/10.1098/rstb.2013.0165, 2013.

834   Fu, B., Li, S., Yu, X., Yang, P., Yu, G., Feng, R., and Zhuang, X.: Chinese ecosystem

835   research network: Progress and perspectives, Ecol. Complex., 7, 225-233,

836   https://doi.org/10.1016/j.ecocom.2010.02.007, 2010.

837   Fu, J. S., Carmichael, G. R., Dentener, F., Aas, W., Andersson, C., Barrie, L. A., Cole,

838   A., Galy-Lacaux, C., Geddes, J., Itahashi, S., Kanakidou, M., Labrador, L., Paulot,

839   F., Schwede, D., Tan, J., and Vet, R.: Improving Estimates of Sulfur, Nitrogen, and

840   Ozone Total Deposition through Multi-Model and Measurement-Model Fusion

841   Approaches, Environ. Sci. Technol., https://doi.org/10.1021/acs.est.1c05929, 2022.

842   He, H., Wang, Y., Ma, Q., Ma, J., Chu, B., Ji, D., Tang, G., Liu, C., Zhang, H., and Hao,

843   J.: Mineral dust and NO_X promote the conversion of SO_2 to sulfate in heavy

844   pollution days, Sci. Rep., 4, 4172, https://doi.org/10.1038/srep04172, 2014.

845   Holland, E. A., Braswell, B. H., Sulzman, J., and Lamarque, J. F.: Nitrogen deposition

846   onto the United States and Western Europe: synthesis of observations and models,

847   Ecol. Appl., 15, 38-57, 2005.

848   Hou, Y., Wang, L., Zhou, Y., Wang, S., Liu, W., and Zhu, J.: Analysis of the
849   tropospheric column nitrogen dioxide over China based on satellite observations
850   during 2008–2017, Atmos. Pollut. Res., 10, 651-655,
851   https://doi.org/10.1016/j.apr.2018.11.003, 2019.

852   Jia, Y., Yu, G., Gao, Y., He, N., Wang, Q., Jiao, C., and Zuo, Y.: Global inorganic
853   nitrogen dry deposition inferred from ground- and space-based measurements, Sci
854   Rep, 6, 19810, https://doi.org/10.1038/srep19810, 2016.

855   Kang, Y., Liu, M., Song, Y., Huang, X., Yao, H., Cai, X., Zhang, H., Kang, L., Liu, X.,
856   Yan, X., He, H., Zhang, Q., Shao, M., and Zhu, T.: High-resolution ammonia
857   emissions inventories in China from 1980 to 2012, Atmos. Chem. Phys., 16,
858   2043-2058, https://doi.org/10.5194/acp-16-2043-2016, 2016.

859   Karplus, V. J., Zhang, S., and Almond, D.: Quantifying coal power plant responses to
860   tighter SO_2 emissions standards in China, Proc. Natl. Acad. Sci., 115, 7004-7009,
861   https://doi.org/10.1073/pnas.1800605115, 2018.

862   Keller, C. A., Long, M. S., Yantosca, R. M., Da Silva, A. M., Pawson, S., and Jacob, D.
863   J.: HEMCO v1.0: a versatile, ESMF-compliant component for calculating
864   emissions in atmospheric models, Geosci. Model Dev., 7, 1409-1417,
865   https://doi.org/10.5194/gmd-7-1409-2014, 2014.

866   Keresztesi, Á., Birsan, M.-V., Nita, I.-A., Bodor, Z., and Szép, R.: Assessing the
867   neutralisation, wet deposition and source contributions of the precipitation
868   chemistry over Europe during 2000–2017, Environ. Sci. Eur., 31,
869   https://doi.org/10.1186/s12302-019-0234-9, 2019.

870   Krotkov, N.A., Lamsal, L.N., Marchenko, S.V., Celarier, E.A., J.Bucsela, E., Swartz,
871   W.H., Joiner, J., team, t.O.c.: OMI/Aura NO_2 Cloud-Screened Total and

Tropospheric Column L3 Global Gridded 0.25 degree × 0.25 degree V3. NASA Goddard Space Flight Center, Goddard Earth Sciences Data and Information Services Center (GES DISC). https://doi.org/10.5067/Aura/OMI/DATA/DATA3007, 2019.

Krotkov, N. A., McLinden, C. A., Li, C., Lamsal, L. N., Celarier, E. A., Marchenko, S. V., Swartz, W. H., Bucsela, E. J., Joiner, J., Duncan, B. N., Boersma, K. F., Veefkind, J. P., Levelt, P. F., Fioletov, V. E., Dickerson, R. R., He, H., Lu, Z., and Streets, D. G.: Aura OMI observations of regional SO_2 and NO_2 pollution changes from 2005 to 2015, Atmos. Chem. Phys., 16, 4605-4629, https://doi.org/10.5194/acp-16-4605-2016, 2016.

Kuang, F., Liu, X., Zhu, B., Shen, J., Pan, Y., Su, M., and Goulding, K.: Wet and dry nitrogen deposition in the central Sichuan Basin of China, Atmos. Environ., 143, 39-50, https://doi.org/10.1016/j.atmosenv.2016.08.032, 2016.

Kuhn, M.: caret: Classification and Regression Training. R package version 6.0-90. https://CRAN.R-project.org/package=caret, 2021.

Li, J.: Pollution trends in China from 2000 to 2017: A multi-sensor view from space, Remote Sens., 12, 208, https://doi.org/10.3390/rs12020208, 2020.

Li, M., Klimont, Z., Zhang, Q., Martin, R. V., Zheng, B., Heyes, C., Cofala, J., Zhang, Y., and He, K.: Comparison and evaluation of anthropogenic emissions of SO_2 and NO_X over China, Atmos. Chem. Phys., 18, 3433-3456, https://doi.org/10.5194/acp-18-3433-2018, 2018.

Li, M., Liu, H., Geng, G., Hong, C., Liu, F., Song, Y., Tong, D., Zheng, B., Cui, H., Man, H., Zhang, Q., and He, K.: Anthropogenic emission inventories in China: a review, Natl. Sci. Rev, 4, 834-866, https://doi.org/10.1093/nsr/nwx150, 2017.

Li, R., Cui, L., Meng, Y., Zhao, Y., and Fu, H.: Satellite-based prediction of daily SO_2

897   exposure across China using a high-quality random forest-spatiotemporal Kriging

898   (RF-STK) model for health risk assessment, Atmos. Environ., 208, 10-19,

899   https://doi.org/10.1016/j.atmosenv.2019.03.029, 2019.

900 Li, R., Cui, L., Fu, H., Zhao, Y., Zhou, W., and Chen, J.: Satellite-Based Estimates of

901   Wet Ammonium (NH_4-N) Deposition Fluxes Across China during 2011-2016

902   Using a Space-Time Ensemble Model, Environ. Sci. Technol., 54, 13419-13428,

903   https://doi.org/10.1021/acs.est.0c03547, 2020a.

904 Li, R., Cui, L., Liang, J., Zhao, Y., Zhang, Z., and Fu, H.: Estimating historical SO_2

905   level across the whole China during 1973-2014 using random forest model,

906   Chemosphere, 247, 125839, https://doi.org/10.1016/j.chemosphere.2020.125839,

907   2020b.

908 Li, Y., Schichtel, B. A., Walker, J. T., Schwede, D. B., Chen, X., Lehmann, C. M. B.,

909   Puchalski, M. A., Gay, D. A., and Collett, J. L., Jr.: Increasing importance of

910   deposition of reduced nitrogen in the United States, Proc. Natl. Acad. Sci., 113,

911   5874-5879, https://doi.org/10.1073/pnas.1525736113, 2016.

912 Likens, G. E., Butler, T. J., Claybrooke, R., Vermeylen, F., and Larson, R.: Long-term

913   monitoring of precipitation chemistry in the U.S.: Insights into changes and

914   condition, Atmos. Environ., 245, 118031,

915   https://doi.org/10.1016/j.atmosenv.2020.118031, 2021.

916 Liu, F., Zhang, Q., Tong, D., Zheng, B., Li, M., Huo, H., and He, K. B.: High-

917   resolution inventory of technologies, activities, and emissions of coal-fired power

918   plants in China from 1990 to 2010, Atmos. Chem. Phys., 15, 13299-13317,

919   https://doi.org/10.5194/acp-15-13299-2015, 2015.

920 Liu, L., Zhang, X., Xu, W., Liu, X., Lu, X., Wang, S., Zhang, W., and Zhao, L.: Ground

921   Ammonia Concentrations over China Derived from Satellite and Atmospheric

922   Transport Modeling, Remote Sens., 9, 467, https://doi.org/10.3390/rs9050467,

923   2017a.

924   Liu, L., Zhang, X., Xu, W., Liu, X., Lu, X., Chen, D., Zhang, X., Wang, S., and Zhang,

925   W.: Estimation of monthly bulk nitrate deposition in China based on satellite NO_2

926   measurement by the Ozone Monitoring Instrument, Remote Sens. Environ., 199,

927   93-106, https://doi.org/10.1016/j.rse.2017.07.005, 2017b.

928   Liu, L., Xu, W., Lu, X., Zhong, B., Guo, Y., Lu, X., Zhao, Y., He, W., Wang, S., Zhang,

929   X., Liu, X., and Vitousek, P.: Exploring global changes in agricultural ammonia

930   emissions and their contribution to nitrogen deposition since 1980, Proc. Natl.

931   Acad. Sci., 119, e2121998119, https://doi.org/10.1073/pnas.2121998119, 2022.

932   Liu, M., Huang, X., Song, Y., Xu, T., Wang, S., Wu, Z., Hu, M., Zhang, L., Zhang, Q.,

933   Pan, Y., Liu, X., and Zhu, T.: Rapid SO_2 emission reductions significantly increase

934   tropospheric ammonia concentrations over the North China Plain, Atmos. Chem.

935   Phys., 18, 17933-17943, https://doi.org/10.5194/acp-18-17933-2018, 2018.

936   Liu, M. Y., Lin, J. T., Boersma, K. F., Pinardi, G., Wang, Y., Chimot, J., Wagner, T., Xie,

937   P. H., Eskes, H., Van Roozendael, M., Hendrick, F., Wang, P. C., Wang, T., Yan, Y.

938   Y., Chen, L. L., and Ni, R. J.: Improved aerosol correction for OMI tropospheric

939   NO_2 retrieval over East Asia: constraint from CALIOP aerosol vertical profile,

940   Natl. Sci. Rev, 12, 1-21, https://doi.org/10.5194/amt-12-1-2019, 2019.

941   Liu, X.J., Zhang, Y., Han, W.X., Tang, A.H., Shen, J.L., Cui, Z.L., Vitousek, P.,

942   Erisman, J.W., Goulding, K., Christie, P., Fangmeier, A., and Zhang, F.S.:

943   Enhanced   nitrogen   deposition   over   China.   Nature   494,   459-462,

944   https://doi.org/10.1038/nature11917, 2013.

945   Liu, X. J., Xu, W., Du, E. Z., Tang, A. H., Zhang, Y., Wen, Z., Hao, T. X., Pan, Y. P.,

946   Zhang, L., Zhao, Y., Shen, J. L., Zhou, F., Gao, Z. L., Chang, Y. H., Goulding, K.,

947   Collett, J. L., Jr., Vitousek, P. M., Zhang, F. S., Zhang, Y. Y., Gu, B. J., and Feng,

948   Z. Z.: Environmental impacts of nitrogen emissions in China and the role of

949　policies in emission reduction, Philos. Trans. Royal Soc., 378,

950　https://doi.org/10.1098/rsta.2019.0324, 2020.

951　Lu, X., Ye, X., Zhou, M., Zhao, Y., Weng, H., Kong, H., Li, K., Gao, M., Zheng, B.,

952　　Lin, J., Zhou, F., Zhang, Q., Wu, D., Zhang, L., and Zhang, Y.: The

953　　underappreciated role of agricultural soil nitrogen oxide emissions in ozone

954　　pollution regulation in North China, Nat. Commun., 12, 5021,

955　　https://doi.org/10.1038/s41467-021-25147-9, 2021.

956　Luo, X., Pan, Y., Goulding, K., Zhang, L., Liu, X., and Zhang, F.: Spatial and seasonal

957　　variations of atmospheric sulfur concentrations and dry deposition at 16 rural and

958　　suburban sites in China, Atmos. Environ., 146, 79-89,

959　　https://doi.org/10.1016/j.atmosenv.2016.07.038, 2016.

960　Lye, C. and Tian, H.: Spatial and temporal patterns of nitrogen deposition in China:

961　　Synthesis of observational data, J. Geophys. Res., 112,

962　　https://doi.org/10.1029/2006jd007990, 2007.

963　Pan, Y. P., Wang, Y. S., Tang, G. Q., and Wu, D.: Wet and dry deposition of

964　　atmospheric nitrogen at ten sites in Northern China, Atmos. Chem. Phys., 12,

965　　6515-6535, https://doi.org/10.5194/acp-12-6515-2012, 2012.

966　Park, R. J.: Natural and transboundary pollution influences on sulfate-nitrate-

967　　ammonium aerosols in the United States: Implications for policy, J. Geophys. Res.,

968　　109, https://doi.org/10.1029/2003jd004473, 2004.

969　Payne, R. J., Stevens, C. J., Dise, N. B., Gowing, D. J., Pilkington, M. G., Phoenix, G.

970　　K., Emmett, B. A., and Ashmore, M. R.: Impacts of atmospheric pollution on the

971　　plant communities of British acid grasslands, Environ. Pollut., 159, 2602-2608,

972　　https://doi.org/10.1016/j.envpol.2011.06.009, 2011.

973　Qin, K., Han, X., Li, D., Xu, J., Loyola, D., Xue, Y., Zhou, X., Li, D., Zhang, K., and

974   Yuan, L.: Satellite-based estimation of surface NO_2 concentrations over east-

975   central China: A comparison of POMINO and OMNO2d data, Atmos. Environ.,

976   224, 117322, https://doi.org/10.1016/j.atmosenv.2020.117322, 2020.

977 Qu, Z., Henze, D. K., Li, C., Theys, N., Wang, Y., Wang, J., Wang, W., Han, J., Shim,

978   C., Dickerson, R. R., and Ren, X.: SO_2 Emission Estimates Using OMI SO_2

979   Retrievals for 2005–2017, J. Geophys. Res.: Atmospheres, 124, 8336-8359,

980   https://doi.org/10.1029/2019jd030243, 2019.

981 Reuss, J. O., Cosby, B. J., and Wright, R. F.: Chemical processes governing soil and

982   water acidification, Nature, 329, 27-32, https://www.nature.com/articles/329027a0,

983   1987.

984 Simpson, D., Benedictow, A., Berge, H., Bergström, R., Emberson, L. D., Fagerli, H.,

985   Flechard, C. R., Hayman, G. D., Gauss, M., Jonson, J. E., Jenkin, M. E., Nyíri, A.,

986   Richter, C., Semeena, V. S., Tsyro, S., Tuovinen, J. P., Valdebenito, Á., and Wind,

987   P.: The EMEP MSC-W chemical transport model – technical description, Atmos.

988   Chem. Phys., 12, 7825-7865, https://doi.org/10.5194/acp-12-7825-2012, 2012.

989 Skyllakou, K., Rivera, P. G., Dinkelacker, B., Karnezi, E., Kioutsioukis, I., Hernandez,

990   C., Adams, P. J., and Pandis, S. N.: Changes in $PM_{2.5}$; concentrations and their

991   sources in the US from 1990 to 2010, Atmos. Chem. Phys., 21, 17115-17132,

992   https://doi.org/10.5194/acp-21-17115-2021, 2021.

993 Song, L., Kuang, F., Skiba, U., Zhu, B., Liu, X., Levy, P., Dore, A., and Fowler, D.:

994   Bulk deposition of organic and inorganic nitrogen in southwest China from 2008

995   to 2013, Environ. Pollut., 227, 157-166,

996   https://doi.org/10.1016/j.envpol.2017.04.031, 2017.

997 Theobald, M. R., Vivanco, M. G., Aas, W., Andersson, C., Ciarelli, G., Couvidat, F.,

998   Cuvelier, K., Manders, A., Mircea, M., Pay, M.-T., Tsyro, S., Adani, M.,

999   Bergström, R., Bessagnet, B., Briganti, G., Cappelletti, A., amp, apos, Isidoro, M.,

1000   Fagerli, H., Mar, K., Otero, N., Raffort, V., Roustan, Y., Schaap, M., Wind, P., and
1001   Colette, A.: An evaluation of European nitrogen and sulfur wet deposition and
1002   their trends estimated by six chemistry transport models for the period 1990–2010,
1003   Atmos. Chem. Phys., 19, 379-405, https://doi.org/10.5194/acp-19-379-2019, 2019.

1004 Tørseth, K., Aas, W., Breivik, K., Fjæraa, A. M., Fiebig, M., Hjellbrekke, A. G., Lund
1005   Myhre, C., Solberg, S., and Yttri, K. E.: Introduction to the European Monitoring
1006   and Evaluation Programme (EMEP) and observed atmospheric composition
1007   change during 1972–2009, Atmos. Chem. Phys., 12, 5447-5481,
1008   https://doi.org/10.5194/acp-12-5447-2012, 2012.

1009 Totsuka, T., Sase, H., and Shimizu, H.: Major activities of acid deposition monitoring
1010   network in East Asia (EANET) and related studies. In: Plant responses to air
1011   pollution and global change. Springer, pp. 251-259, 2005.

1012 Vet, R., Artz, R. S., Carou, S., Shaw, M., Ro, C.-U., Aas, W., Baker, A., Bowersox, V.
1013   C., Dentener, F., Galy-Lacaux, C., Hou, A., Pienaar, J. J., Gillett, R., Forti, M. C.,
1014   Gromov, S., Hara, H., Khodzher, T., Mahowald, N. M., Nickovic, S., Rao, P. S. P.,
1015   and Reid, N. W.: A global assessment of precipitation chemistry and deposition of
1016   sulfur, nitrogen, sea salt, base cations, organic acids, acidity and pH, and
1017   phosphorus, Atmos. Environ., 93, 3-100,
1018   https://doi.org/10.1016/j.atmosenv.2013.10.060, 2014.

1019 Wang, J., Sha, Z., Zhang, J., Kang, J., Xu, W., Goulding, K., and Liu, X.: Reactive N
1020   emissions from cropland and their mitigation in the North China Plain, Environ.
1021   Res., 214, 114015, https://doi.org/10.1016/j.envres.2022.114015, 2022.

1022 Wen, Z., Xu, W., Li, Q.Q., Han, M.J., Tang, A.H., Zhang, Y., Luo, X.S., Shen, J.L.,
1023   Wang, W., Li, K.H., Pan, Y.P., Zhang, L., Li, W.Q., Collett Jr, J.L., Zhong, B.Q.,
1024   Wang, X.M., Goulding, K., Zhang, F.S., and Liu, X.J.: Changes of nitrogen
1025   deposition in China from 1980 to 2018. Environment International 144, 106022,

1026   https://doi.org/10.1016/j.envint.2020.106022, 2020.

1027 Wesely, M. L.: Parameterization of surface resistances to gaseous dry deposition in

1028   regional-scale numerical models, Atmos. Environ., 23, 1293-1304,

1029   https://doi.org/https://doi.org/10.1016/0004-6981(89)90153-4, 1989.

1030 Whitburn, S., Van Damme, M., Clarisse, L., Bauduin, S., Heald, C. L., Hadji-Lazaro, J.,

1031   Hurtmans, D., Zondlo, M. A., Clerbaux, C., and Coheur, P. F.: A flexible and

1032   robust neural network IASI-NH$_3$ retrieval algorithm, J. Geophys. Res.:

1033   Atmospheres, 121, 6581-6599, https://doi.org/10.1002/2016jd024828, 2016.

1034 Wu, Y., Di, B., Luo, Y., Grieneisen, M. L., Zeng, W., Zhang, S., Deng, X., Tang, Y., Shi,

1035   G., Yang, F., and Zhan, Y.: A robust approach to deriving long-term daily surface

1036   NO$_2$ levels across China: Correction to substantial estimation bias in back-

1037   extrapolation, Environ. Int., 154, 106576,

1038   https://doi.org/10.1016/j.envint.2021.106576, 2021.

1039 Xia, Y., Zhao, Y., and Nielsen, C. P.: Benefits of China's efforts in gaseous pollutant

1040   control indicated by the bottom-up emissions and satellite observations 2000–

1041   2014, Atmos. Environ., 136, 43-53,

1042   https://doi.org/10.1016/j.atmosenv.2016.04.013, 2016.

1043 Xu, W., Zhang, L., and Liu, X.: A database of atmospheric nitrogen concentration and

1044   deposition from the nationwide monitoring network in China, Sci. Data, 6, 51,

1045   https://doi.org/10.1038/s41597-019-0061-2, 2019.

1046 Xu, W., Liu, L., Cheng, M., Zhao, Y., Zhang, L., Pan, Y., Zhang, X., Gu, B., Li, Y.,

1047   Zhang, X., Shen, J., Lu, L., Luo, X., Zhao, Y., Feng, Z., Collett Jr, J. L., Zhang, F.,

1048   and Liu, X.: Spatial–temporal patterns of inorganic nitrogen air concentrations

1049   and deposition in eastern China, Atmos. Chem. Phys., 18, 10931-10954,

1050   https://doi.org/10.5194/acp-18-10931-2018, 2018.

1051 Xu, W., Luo, X. S., Pan, Y. P., Zhang, L., Tang, A. H., Shen, J. L., Zhang, Y., Li, K. H.,
1052 Wu, Q. H., Yang, D. W., Zhang, Y. Y., Xue, J., Li, W. Q., Li, Q. Q., Tang, L., Lu, S.
1053 H., Liang, T., Tong, Y. A., Liu, P., Zhang, Q., Xiong, Z. Q., Shi, X. J., Wu, L. H.,
1054 Shi, W. Q., Tian, K., Zhong, X. H., Shi, K., Tang, Q. Y., Zhang, L. J., Huang, J. L.,
1055 He, C. E., Kuang, F. H., Zhu, B., Liu, H., Jin, X., Xin, Y. J., Shi, X. K., Du, E. Z.,
1056 Dore, A. J., Tang, S., Collett, J. L., Goulding, K., Sun, Y. X., Ren, J., Zhang, F. S.,
1057 and Liu, X. J.: Quantifying atmospheric nitrogen deposition through a nationwide
1058 monitoring network across China, Atmos. Chem. Phys., 15, 12345-12360,
1059 https://doi.org/10.5194/acp-15-12345-2015, 2015.

1060 Xu, X.: China's GDP and POP spatial distribution kilometer grid dataset. Resources
1061 and environment science data registration and publication system
1062 (http://www.resdc.cn/DOI), 2017.

1063 Yamaga, S., Ban, S., Xu, M., Sakurai, T., Itahashi, S., and Matsuda, K.: Trends of
1064 sulfur and nitrogen deposition from 2003 to 2017 in Japanese remote areas,
1065 Environ. Pollut., 289, 117842, https://doi.org/10.1016/j.envpol.2021.117842, 2021.

1066 Ye, C., Lu, K., Song, H., Mu, Y., Chen, J., and Zhang, Y.: A critical review of sulfate
1067 aerosol formation mechanisms during winter polluted periods, J. Environ. Sci. (China),
1068 123, 387-399, https://doi.org/10.1016/j.jes.2022.07.011, 2023.

1069 Yu, G., Jia, Y., He, N., Zhu, J., Chen, Z., Wang, Q., Piao, S., Liu, X., He, H., Guo, X.,
1070 Wen, Z., Li, P., Ding, G., and Goulding, K.: Stabilization of atmospheric nitrogen
1071 deposition in China over the past decade, Nature Geosci., 12, 424-431,
1072 https://doi.org/10.1038/s41561-019-0352-4, 2019.

1073 Zhan, X., Yu, G., He, N., Jia, B., Zhou, M., Wang, C., Zhang, J., Zhao, G., Wang, S.,
1074 Liu, Y., and Yan, J.: Inorganic nitrogen wet deposition: Evidence from the North-
1075 South Transect of Eastern China, Environ. Pollut., 204, 1-8,
1076 https://doi.org/10.1016/j.envpol.2015.03.016, 2015.

1077 Zhang, G., Pan, Y., Tian, S., Cheng, M., Xie, Y., Wang, H., and Wang, Y.: Limitations
1078   of passive sampling technique of rainfall chemistry and wet deposition flux
1079   characterization, Res. Environ., 28, 684-690, https://doi.org/10.13198/j.issn.1001-
1080   6929.2015.05.03, 2015.

1081 Zhang, L., Gong, S., Padro, J., and Barrie, L.: A size-segregated particle dry deposition
1082   scheme for an atmospheric aerosol module, Atmos. Environ., 35, 549-560,
1083   https://doi.org/10.1016/S1352-2310(00)00326-5, 2001.

1084 Zhang, Q., Zheng, Y., Tong, D., Shao, M., Wang, S., Zhang, Y., Xu, X., Wang, J., He,
1085   H., Liu, W., Ding, Y., Lei, Y., Li, J., Wang, Z., Zhang, X., Wang, Y., Cheng, J., Liu,
1086   Y., Shi, Q., Yan, L., Geng, G., Hong, C., Li, M., Liu, F., Zheng, B., Cao, J., Ding,
1087   A., Gao, J., Fu, Q., Huo, J., Liu, B., Liu, Z., Yang, F., He, K., and Hao, J.: Drivers
1088   of improved $PM_{2.5}$ air quality in China from 2013 to 2017, Proc. Natl. Acad. Sci.,
1089   116, 24463-24469, https://doi.org/10.1073/pnas.1907956116, 2019.

1090 Zhang, T., Chen, H. Y. H., and Ruan, H.: Global negative effects of nitrogen deposition
1091   on soil microbes, ISME J, 12, 1817-1825, https://doi.org/10.1038/s41396-018-
1092   0096-y, 2018a.

1093 Zhang, X. Y., Chuai, X. W., Liu, L., Zhang, W. T., Lu, X. H., Zhao, L. M., and Chen, D.
1094   M.: Decadal trends in wet sulfur deposition in China estimated from OMI SO_2
1095   columns, J. Geophys. Res. (Atmos.), 123, 10796-10811,
1096   https://doi.org/10.1029/2018jd028770, 2018b.

1097 Zhang, Y., Liu, X. J., Fangmeier, A., Goulding, K. T. W., and Zhang, F. S.: Nitrogen
1098   inputs and isotopes in precipitation in the North China Plain, Atmos. Environ., 42,
1099   1436-1448, https://doi.org/10.1016/j.atmosenv.2007.11.002, 2008.

1100 Zhang, Y., Zhao, J., and Yin, H.: European Union agricultural policy transformation
1101   trend and enlightenment, World Agriculture, 05, 2020. (in Chinese)

1102 Zhao, S. and Qiao, G.: The shadow prices of CO_2, SO_2 and NO_X for U.S. coal power

1103 industry 2010–2017: a convex quantile regression method, J. Productiv. Anal., 57,

1104 243-253, https://doi.org/10.1007/s11123-022-00629-0, 2022.

1105 Zhao, Y., Xi, M., Zhang, Q., Dong, Z., Ma, M., Zhou, K., Xu, W., Xing, J., Zheng, B.,

1106 Wen, Z., Liu, X., Nielsen, C. P., Liu, Y., Pan, Y., and Zhang, L.: Decline in bulk

1107 deposition of air pollutants in China lags behind reductions in emissions, Nature

1108 Geosci., 15, 190-195, https://doi.org/10.1038/s41561-022-00899-1, 2022.

1109 Zheng, B., Tong, D., Li, M., Liu, F., Hong, C., Geng, G., Li, H., Li, X., Peng, L., Qi, J.,

1110 Yan, L., Zhang, Y., Zhao, H., Zheng, Y., He, K., and Zhang, Q.: Trends in China's

1111 anthropogenic emissions since 2010 as the consequence of clean air actions,

1112 Atmos. Chem. Phys., 18, 14095-14111, https://doi.org/10.5194/acp-18-14095-

1113 2018, 2018a.

1114 Zheng, X. D., Liu, X. Y., Song, W., Sun, X. C., and Liu, C. Q.: Nitrogen isotope

1115 variations of ammonium across rain events: Implications for different scavenging

1116 between ammonia and particulate ammonium, Environ. Pollut., 239, 392-398,

1117 https://doi.org/10.1016/j.envpol.2018.04.015, 2018b.

1118 Zhou, K., Zhao, Y., Zhang, L., and Xi, M.: Declining dry deposition of NO_2 and SO_2

1119 with diverse spatiotemporal patterns in China from 2013 to 2018, Atmos. Environ.,

1120 262, 118655, https://doi.org/10.1016/j.atmosenv.2021.118655, 2021.

1121 Zhu, J., He, N., Wang, Q., Yuan, G., Wen, D., Yu, G., and Jia, Y.: The composition,

1122 spatial patterns, and influencing factors of atmospheric wet nitrogen deposition in

1123 Chinese terrestrial ecosystems, Sci. Total Environ., 511, 777-785,

1124 https://doi.org/10.1016/j.scitotenv.2014.12.038, 2015.

1125

Figure captions

Figure 1 The research domain of this study. The pink points represent China National

Environmental Monitoring Centre (CNEMC) and the green points represent

Nationwide Nitrogen Deposition Monitoring Network (NNDMN). The Qinling-Huaihe

Line is the boundary between the north and the south of the country. The map data

provided by Resource and Environment Data Cloud Platform are freely available for

academic use (http://www.resdc.cn/data.aspx?DATAID=201), © Institute of

Geographic Sciences & Natural Resources Research, Chinese Academy of Sciences.

Figure 2 Methodology framework to estimate dry and wet deposition of this study. The

blue process shows the four steps to establish the RF model. The orange process shows

the three steps in establishing a GAM model. See Sections 2.2 to 2.3 of the method

section in the text for the acquisition of the preliminary data set.

Figure 3 Comparison of deposition between this study and other literatures for dry (a),

wet (b) and total deposition (c). The black cross and the pentagram are the average of

literature-reported results and the multi-year average of this study, respectively. The

boxplots represent the dispersion of deposition collected from literatures. The central

horizontal line, the upper side line, and the lower side line of the box represent the

median value, the upper quartile (75th Quantile, Q3) and the lower quartile (25th

Quantile, Q1). The vertical line extending out of the box represents 1.5 times the

interquartile interval (IQR, i.e., Q3-Q1), and the horizontal lines represent the upper

limit (Q3+1.5IQR) and the lower limit (Q1-1.5 IQR).

Figure 4 Contribution of different forms and species to the estimated total N and S

deposition in China.

Figure 5 The interannual variability of N and S deposition, emissions and component

proportion in China from 2005 to 2020. The emission data over China were taken from

MEIC.

Figure 6 The interannual variations of emissions, deposition and RDN/OXN for China,

28 Europe countries (EU) and the USA. All the data are relative to the 2005 levels. The

grey dotted lines are a visual guidance for 1.0 on each of the y axes. (a) NO_X emissions

and OXN deposition; (b) NH_3 emissions and RDN deposition; (c) SO_2 emissions and

1156 sulfur deposition; and (d) RDN/OXN. The emission data were respectively taken from

1157 MEIC, the European Environment Agency (EEA,

1158 https://www.eea.europa.eu/themes/air), and U.S. Environmental Protection Agency

1159 (EPA, https://www.epa.gov/air-emissions-inventories/air-pollutant-emissionstrends-

1160 data, while deposition data from European Monitoring and Evaluation Programme

1161 (EMEP, https://projects.nilu.no/ccc/index.html) for Europe and Clean Air Status and

1162 Trends Network (CASTNET, https://www.epa.gov/castnet) and National Atmospheric

1163 Deposition Program (NADP, https://nadp.slh.wisc.edu/networks/national-trends-

1164 network/) for the USA.

1165 Figure 7 The spatial distributions of N and S deposition flux in 2005-2020.

1166 Figure 8 The interannual variations and relative changes of deposition of OXN (a),

1167 RDN (b) and sulfur (c) by region. All the data are relative to the 2005 levels. The

1168 orange line represents eastern China (SE+NC with Inner Mongolia excluded, see

1169 Figure 1 for the region definitions), the blue line represents western China (NW+TP),

1170 and the red line represents the average level of whole China.

1171 Figure 9 Annual mean D/E ratio of OXN, RDN and sulfur from 2005 to 2020 in

1172 different regions (a) and linear relationship between regional deposition and emissions

1173 (b-d).

1174 Figure 10 The spatial distribution of multi-year seasonal variation of the total

1175 deposition across 2005-2020.

1176

Tables

Table 1 Comparison of relative change rates of emissions and deposition in the process of pollution control in China, Europe and the USA. The starting and ending time was selected according to the period of the fastest decline of deposition in China, and the time period of emission decline was selected according to the reference deposition. The emission data were respectively taken from MEIC, the European Environment Agency (EEA, https://www.eea.europa.eu/themes/air), and U.S. Environmental Protection Agency (EPA, https://www.epa.gov/air-emissions-inventories/air-pollutant-emissionstrends-data, while deposition data from European Monitoring and Evaluation Programme (EMEP, https://projects.nilu.no/ccc/index.html) for Europe and Clean Air Status and Trends Network (CASTNET, https://www.epa.gov/castnet) and National Atmospheric Deposition Program (NADP, https://nadp.slh.wisc.edu/networks/national-trends-network/) for the USA.

Relative change	Emissions			
	NO_X		SO_2	
The USA	-35.9%	(2003-2011)	-78.4%	(2003-2016)
Europe	-17.3%	(2000-2008)	-57.6%	(2000-2013)
China	-32.2%	(2012-2020)	-75.5%	(2007-2020)
	Deposition			
	OXN		S	
The USA	-26.0%	(2003-2011)	-72.5%	(2003-2016)
Europe	-11.1%	(2000-2008)	-49.9%	(2000-2013)
China	-7.1%	(2012-2020)	-27.0%	(2007-2020)

1191 **Table 2 The interannual changes in deposition and emissions of N and S by**

1192 **regions for 2005–2020.** Eastern China includes NC (Inner Mongolia excluded) and SE,

1193 and western China includes TP and NW (see Figure 1 for the region definitions). P1

1194 and P2 indicate 2005–2012 and 2012–2020, respectively.

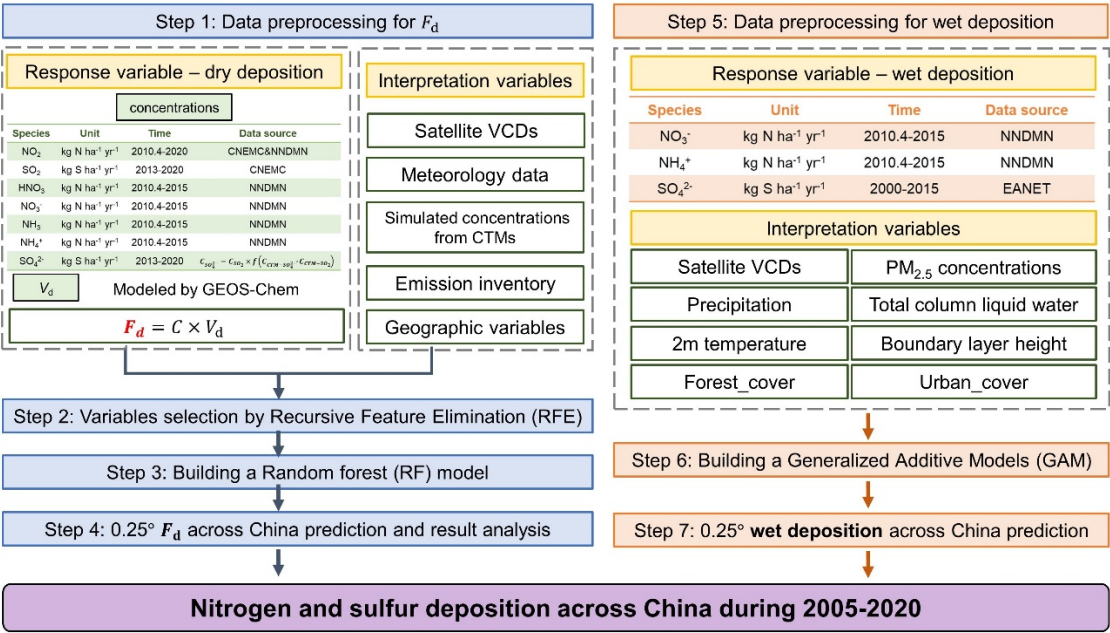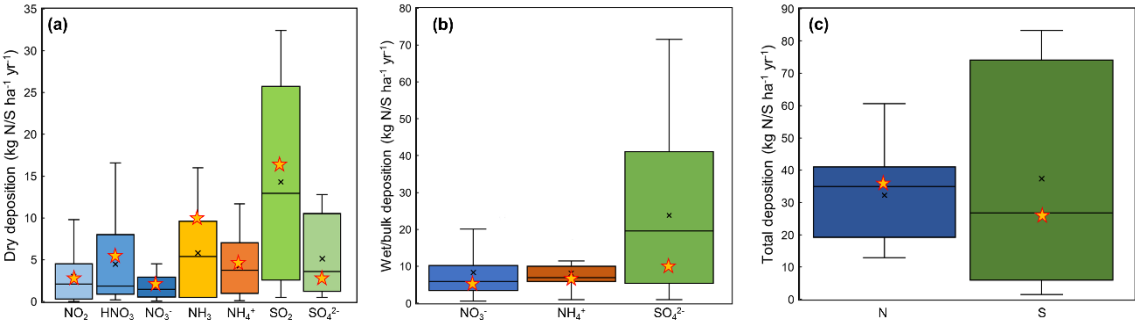| Interannual change (units: kg N/S ha^{-1} yr^{-1})		Whole China		Eastern China		Western China	
		P1	P2	P1	P2	P1	P2
Emissions	NO$_X$	0.60	-0.42	1.12	-1.33	0.63	-0.24
	NH$_3$	0.08	-0.21	0.08	-0.83	0.09	-0.02
	SO$_2$	-0.39	-1.24	-2.98	-4.62	0.01	-0.89
Deposition	Total OXN	0.09	-0.15	0.22	-0.41	0.07	-0.08
	Total RDN	0.05	0.06	0.06	0.28	0.05	0.22
	Total N	0.14	-0.09	0.28	-0.14	0.13	0.14
	Total S	-0.29	-0.82	-0.34	-1.55	-0.29	-0.60
Relative annual change to 2005 (P1) or 2012 (P2)		P1	P2	P1	P2	P1	P2
Emissions	NO$_X$	49%	-31%	17%	-25%	110%	-29%
	NH$_3$	7%	-15%	2%	-22%	17%	-3%
	SO$_2$	-13%	-72%	-25%	-73%	10%	-74%
Deposition	Total OXN	5%	-7%	9%	-12%	4%	-5%
	Total RDN	3%	3%	5%	9%	3%	10%
	Total N	4%	-2%	7%	-2%	3%	1%
	Total S	-7%	-21%	-3%	-28%	-9%	-18%

1195
1196

1197 **Figures**
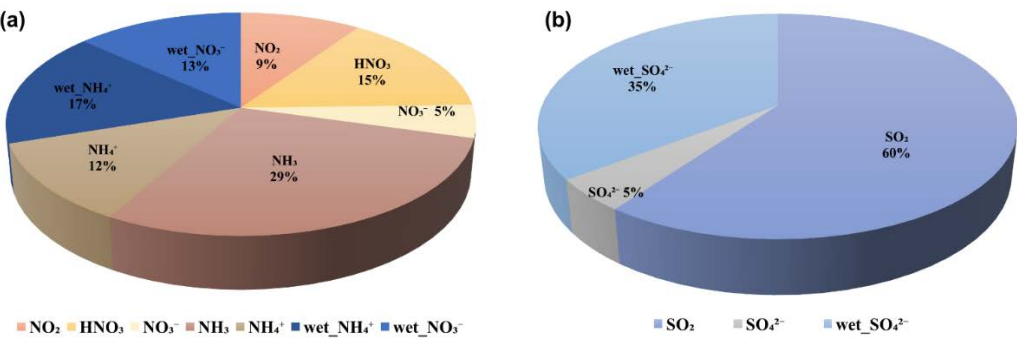
1198 **Figure 1**

1199

1200

1201 **Figure 2**

Step 1: Data preprocessing for F_d		Step 5: Data preprocessing for wet deposition

Response variable – dry deposition

concentrations

Species	Unit	Time	Data source
NO_2	kg N ha^{-1} yr^{-1}	2010.4-2020	CNEMC&NNDMN
SO_2	kg S ha^{-1} yr^{-1}	2013-2020	CNEMC
HNO_3	kg N ha^{-1} yr^{-1}	2010.4-2015	NNDMN
NO_3^-	kg N ha^{-1} yr^{-1}	2010.4-2015	NNDMN
NH_3	kg N ha^{-1} yr^{-1}	2010.4-2015	NNDMN
NH_4^+	kg N ha^{-1} yr^{-1}	2010.4-2015	NNDMN
SO_4^{2-}	kg S ha^{-1} yr^{-1}	2013-2020	$c_{SO_4^{2-}} = c_{SO_2} \times f(c_{CTM \cdot SO_4^{2-}} \cdot c_{CTM-SO_2})$

V_d Modeled by GEOS-Chem

$F_d = C \times V_d$

Interpretation variables

- Satellite VCDs
- Meteorology data
- Simulated concentrations from CTMs
- Emission inventory
- Geographic variables

Response variable – wet deposition

Species	Unit	Time	Data source
NO_3^-	kg N ha^{-1} yr^{-1}	2010.4-2015	NNDMN
NH_4^+	kg N ha^{-1} yr^{-1}	2010.4-2015	NNDMN
SO_4^{2-}	kg S ha^{-1} yr^{-1}	2000-2015	EANET

Interpretation variables

Satellite VCDs	$PM_{2.5}$ concentrations
Precipitation	Total column liquid water
2m temperature	Boundary layer height
Forest_cover	Urban_cover

Step 2: Variables selection by Recursive Feature Elimination (RFE)

Step 3: Building a Random forest (RF) model

Step 4: 0.25° F_d across China prediction and result analysis

Step 6: Building a Generalized Additive Models (GAM)

Step 7: 0.25° **wet deposition** across China prediction

Nitrogen and sulfur deposition across China during 2005-2020

1202
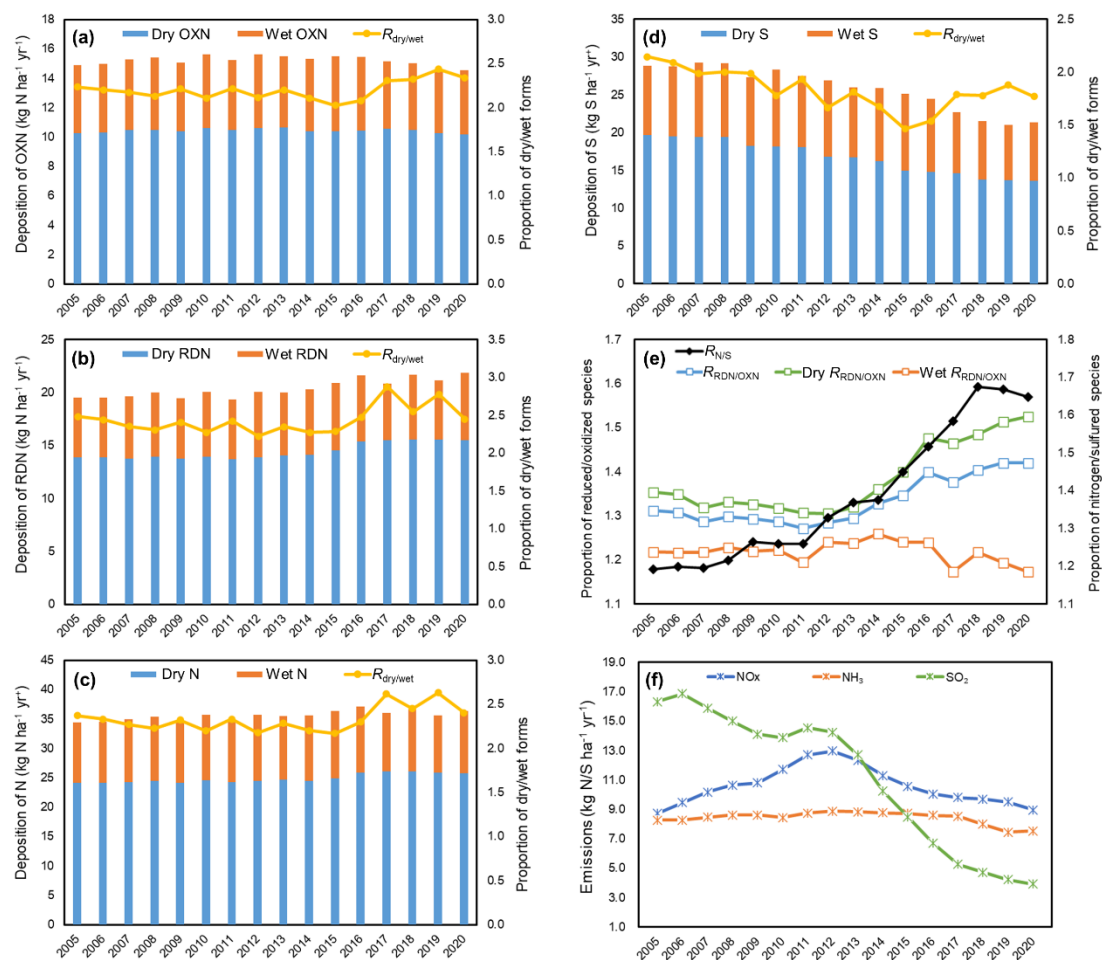1203

Figure 3

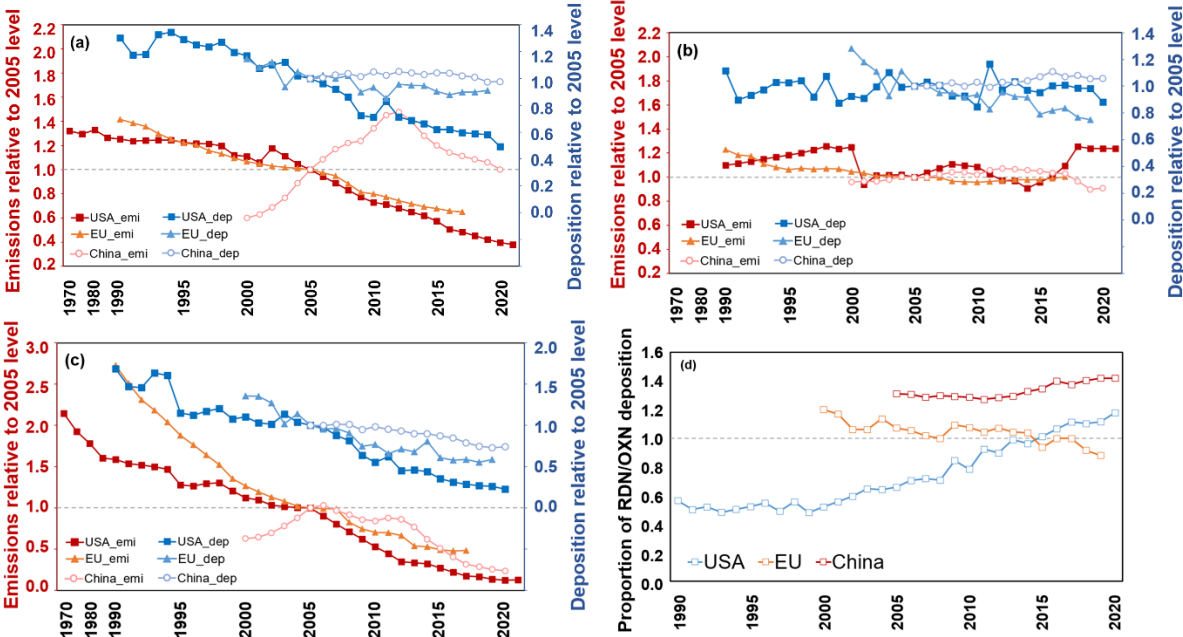1207   **Figure 4**

1208
1209

1210   **Figure 5**

1211

1212

52

1213   **Figure 6**

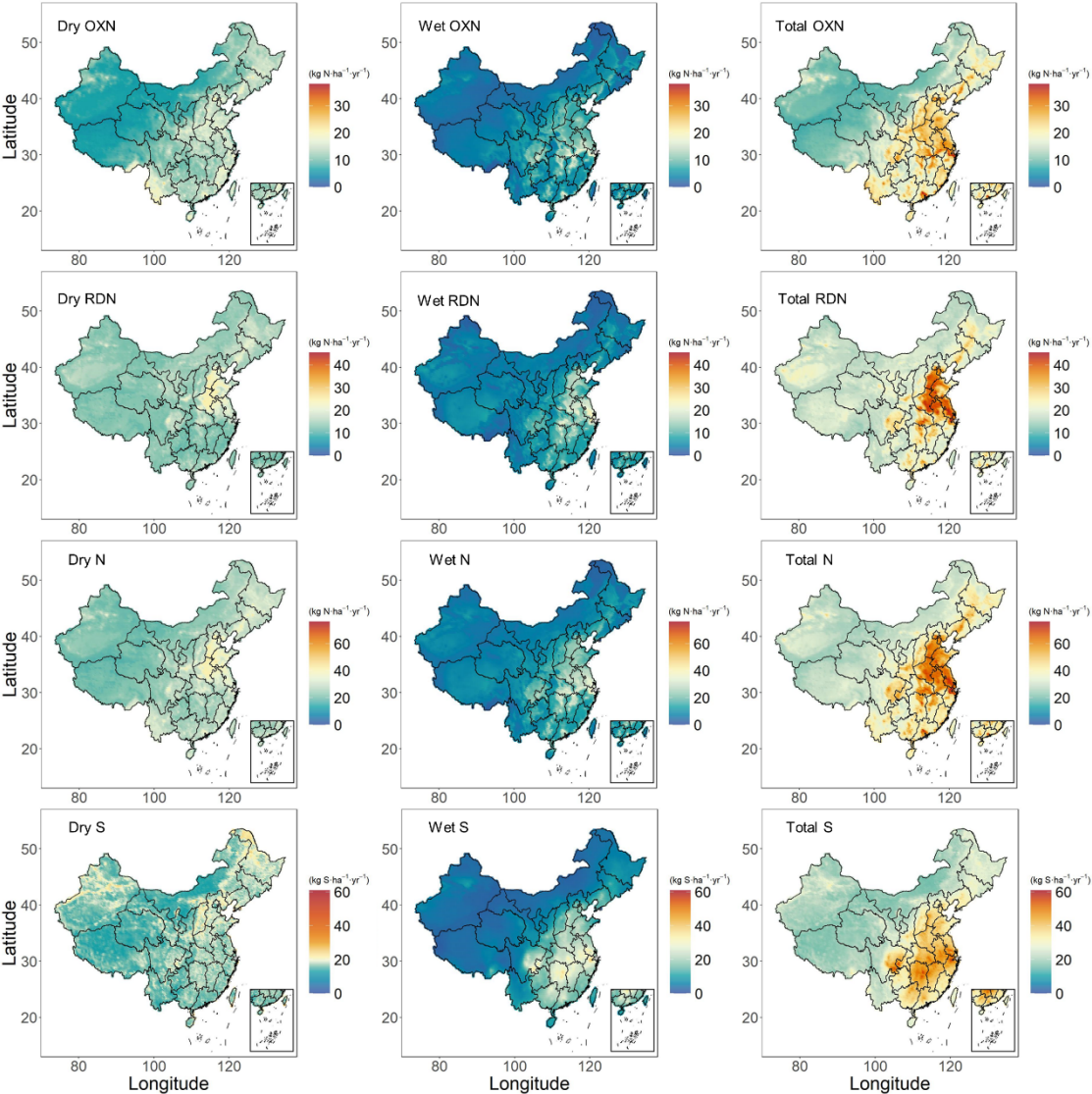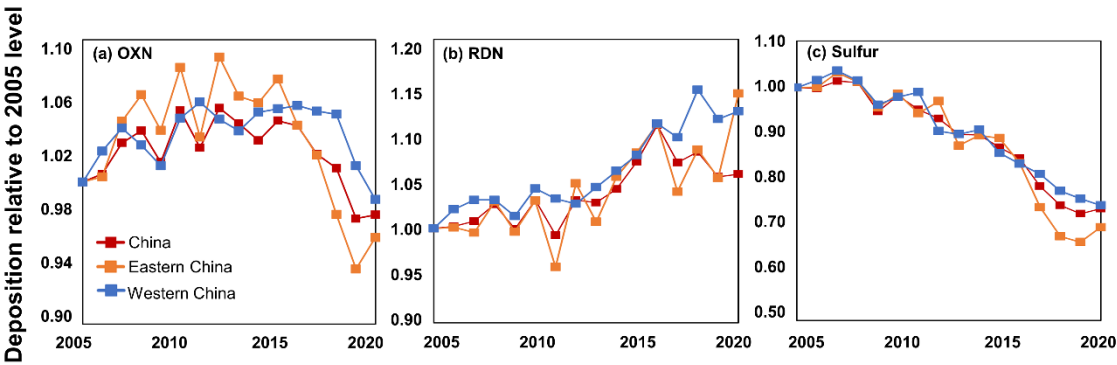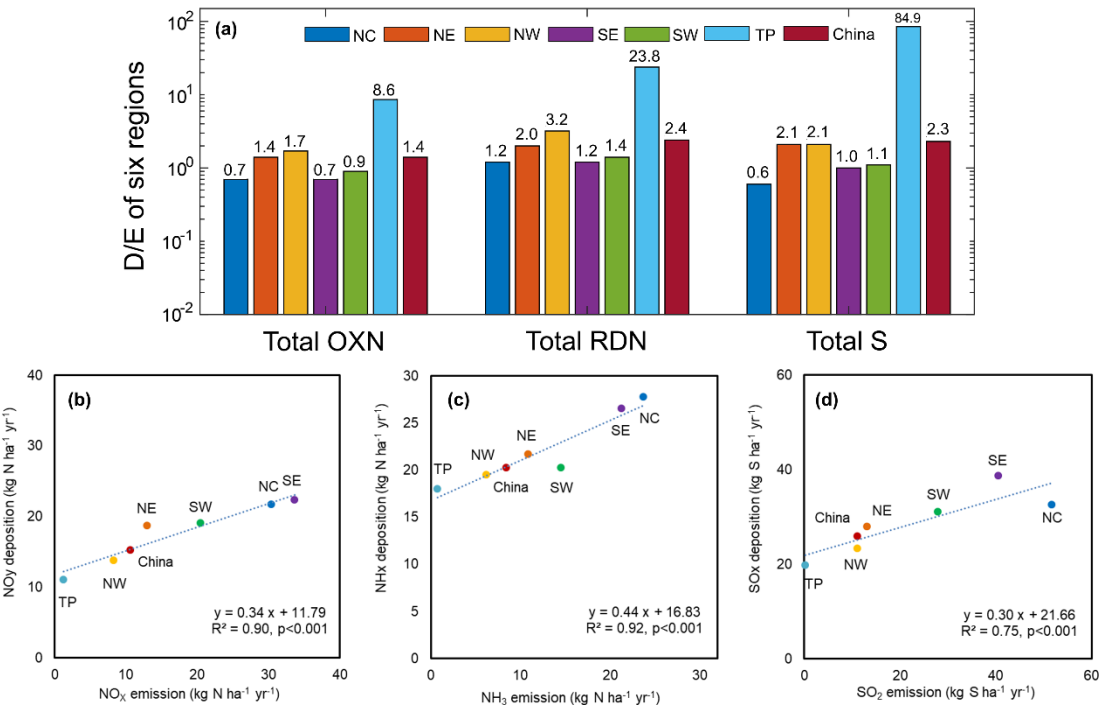1214

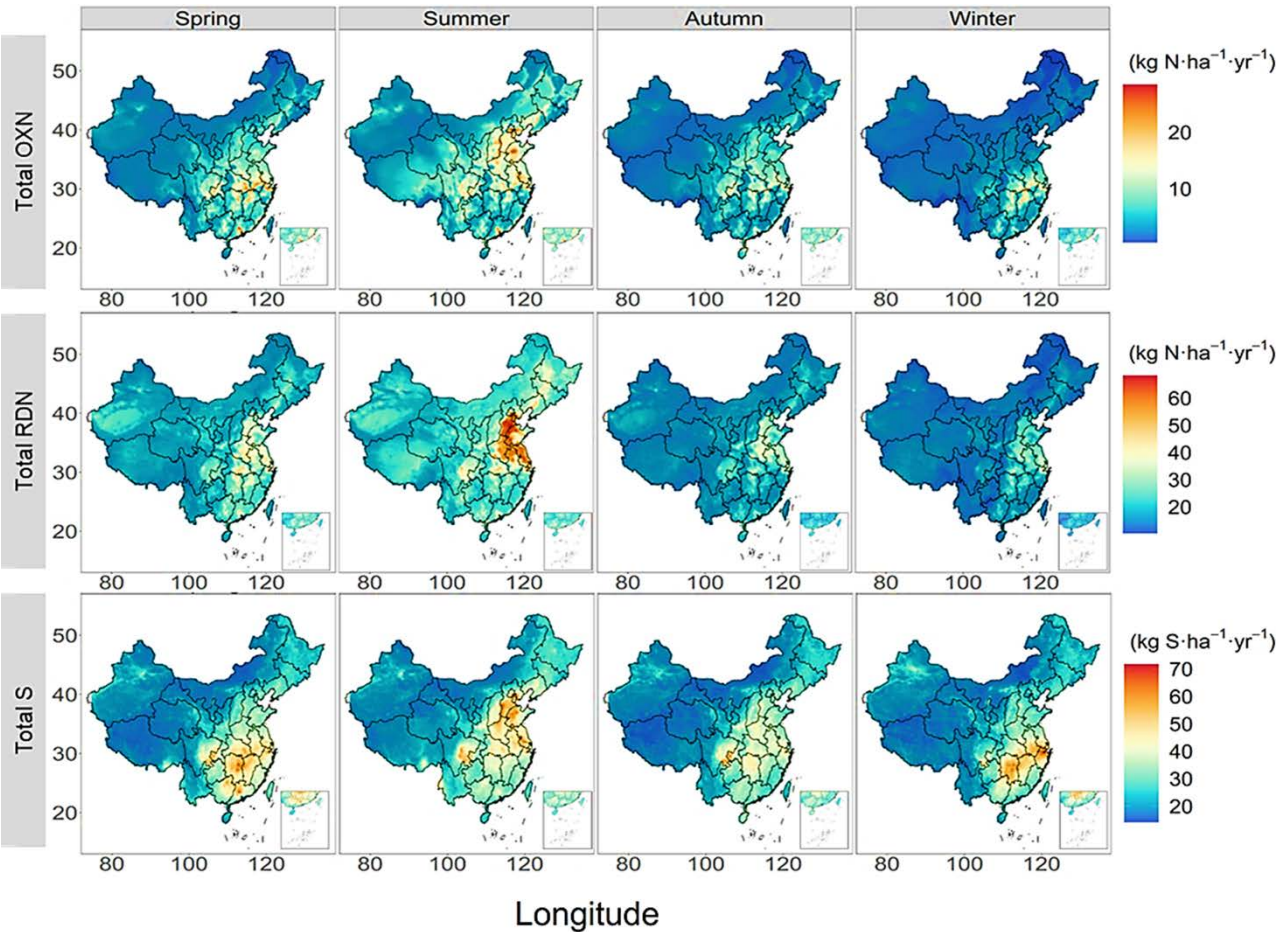1215

1216   **Figure 7**

1217

1218

1219   **Figure 8**

1220

1221

Figure 9

1225   **Figure 10**

1226

1227